iScience

Article

A combinatorial and computational Tandem approach towards a universal therapeutics against ACE2-mediated coronavirus infections

Graphical abstract

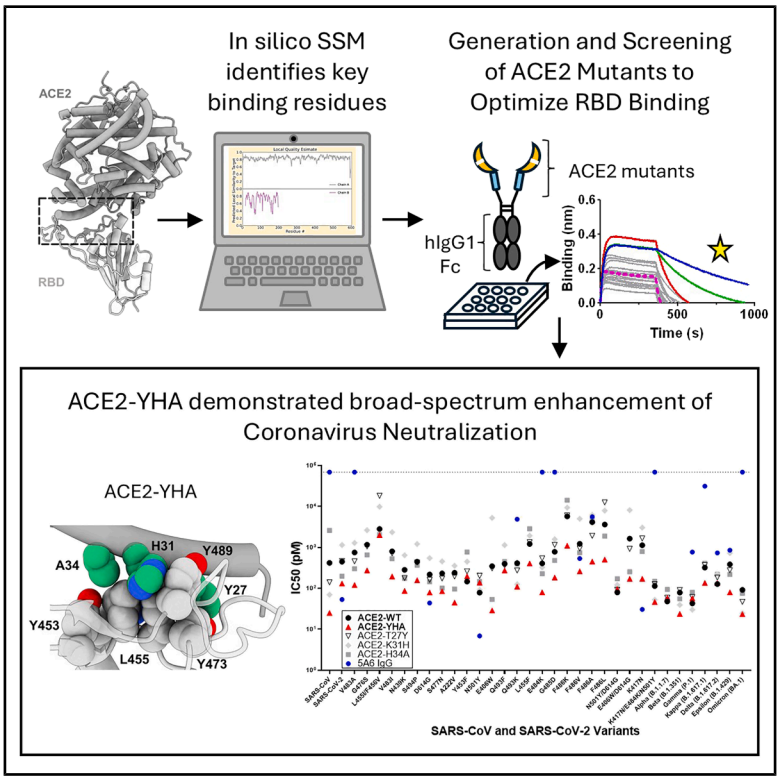

Highlights

- Developed ACE2-YHA, a high-affinity ACE2 decoy with pan-coronavirus potential
- ACE2-YHA shows enhanced binding to SARS-CoV, SARS-CoV-2, and bat SARSr-CoVs
- Demonstrated potent neutralization of SARS-CoV and over 40 SARS-CoV-2 variants
- ACE2-YHA neutralizes SARS-CoV-2 Delta & Omicron variants in human airway epithelia

Authors

Chia Yin Lee, Ching-Wen Huang, Louis De Falco, Jr., ..., Andrés Pizzorno, Roland G. Huber, Cheng-I Wang

Correspondence

wang_chengi@immunol.a-star.edu.sg

In brief

Natural sciences; Biological sciences; Biochemistry; Microbiology; Virology

Lee et al., 2025, iScience *28*, 112687
June 20, 2025
https://doi.org/10.1016/j.isci.2025.112687

CellPress

iScience

CellPress
OPEN ACCESS

Article

A combinatorial and computational Tandem approach towards a universal therapeutics against ACE2-mediated coronavirus infections

Chia Yin Lee,[1,7] Ching-Wen Huang,[1,7] Louis De Falco, Jr.,[2] Rabiatul Adawiyah Minhat,[1] Aurélien Traversier,[3,4,5] Bei Wang,[1] Siti Nazihah Mohd Salleh,[1] Eve Zi Xian Ngoh,[1] Yuling Huang,[6] Jenna Kim,[6] Matthew Zirui Tay,[6] Manuel Rosa-Calatrava,[3,4,5] Andrés Pizzorno,[3,4] Roland G. Huber,[2] and Cheng-I Wang[1,8,*]

[1]Singapore Immunology Network (SIgN), Agency for Science, Technology and Research (A*STAR), 8A Biomedical Grove, Immunos #03-06, Singapore 138648, Republic of Singapore

[2]Bioinformatics Institute (BII), Agency for Science, Technology and Research (A*STAR), 30 Biopolis Street, Matrix #07-01, Singapore 138671, Republic of Singapore

[3]CIRI, Centre International de Recherche en Infectiologie, Team VirPath, INSERM U1111, CNRS UMR 5308, ENS de Lyon, Université Claude Bernard Lyon 1, Lyon, France

[4]International Research Laboratory RESPIVIR France - Canada, Centre de Recherche en Infectiologie, Faculté de Médecine RTH Laennec, 69008 Lyon, France, Université Claude Bernard Lyon 1, Université de Lyon, INSERM, CNRS, ENS de Lyon, France, Centre Hospitalier Universitaire de Québec - Université Laval, Québec, QC G1V 4G2, Canada

[5]VirNext, Faculté de Médecine RTH Laennec, Université Claude Bernard Lyon 1, Université de Lyon, 69008 Lyon, France

[6]Infectious Diseases Labs (ID Labs), Agency for Science, Technology and Research (A*STAR), 8A Biomedical Grove, Immunos #05-13, Singapore 138648, Republic of Singapore

[7]These authors contributed equally

[8]Lead contact

*Correspondence: wang_chengi@immunol.a-star.edu.sg

https://doi.org/10.1016/j.isci.2025.112687

SUMMARY

Angiotensin-converting enzyme 2 (ACE2) receptor plays a pivotal role in the infection of several coronaviruses, including SARS-CoV and SARS-CoV-2. We combined computational and experimental protein engineering approaches to develop ACE2-YHA, a soluble, high-affinity ACE2 decoy with pan-coronavirus preventive and therapeutic potential. Leveraging native human ACE2–SARS-CoV/SARS-CoV-2 receptor binding domain (RBD) complex homology models, we employed *in silico* site-saturation mutagenesis to predict key ACE2-RBD interacting residues. Subsequent generation of ACE2 mutants and high-throughput screening identified specific ACE2 residue substitutions that enhanced binding to both SARS-CoV and SARS-CoV-2 RBDs. The triple mutant ACE2-YHA demonstrated significantly enhanced binding affinity to SARS-CoV, SARS-CoV-2, and bat SARSr-CoVs' RBDs. It effectively neutralized SARS-CoV and numerous SARS-CoV-2 variants with picomolar IC50s in pseudotyped virus assays. Notably, ACE2-YHA displayed potent neutralization against major variants of concern, including Delta and Omicron, in human airway epithelia, positioning it as a promising universal decoy for current and future ACE2-binding coronavirus outbreaks.

INTRODUCTION

Mutation and adaptation have driven the co-evolution of coronaviruses (CoVs) and their hosts, including human beings, for thousands of years. The outbreaks of severe acute respiratory syndrome (SARS) and coronavirus disease 2019 (COVID-19) since the beginning of the 21st century reveal how devastating and life-threatening a human CoV infection can be. SARS-CoV and SARS-CoV-2, the viruses that are responsible for SARS and COVID-19, respectively, are zoonotic coronaviruses originating from bats/palm civets that successfully crossed the species barrier, leading to fatal pneumonia in humans. To be prepared for the continuing threats from the cross-species transmission of coronaviruses, there is an urgent need for readily available therapeutic drugs against various types of coronaviruses for fast responses.

A strategic approach to the development of the anti-coronavirus therapy involves inhibiting the interaction between the virus spike proteins and the host receptors, thereby preventing viral entry. The predominant focus on developing neutralizing antibodies and vaccines against spike proteins since the outbreak of SARS and COVID-19 has encountered challenges due to weakened efficacy against viral mutations that emerged during the pandemic. These mutations often render neutralizing antibodies less effective, given their high specificity to the virus strain used in their development.[1–3] Mutations in the receptor-binding

domain (RBD), the primary target for neutralizing Abs, can modify epitopes, alter the spike protein's structure, and affect RBD conformational dynamics, all of which hinder antibody binding.[4–8] This reduces the ability of existing neutralizing antibodies to block viral entry, resulting in decreased efficacy of vaccines and therapeutic antibodies. To address this issue and minimize the risk of viral escape, we explore the utility of a universal decoy receptor.

Many human and animal coronaviruses, such as SARS-CoV, SARS-CoV-2, Bat SL-CoV-WIV1, Bat-CoV RaTG13, and Pangolin-CoV-2020, are known to utilize host angiotensin-converting enzyme 2 (ACE2) as the entry receptor to infect host cells.[9–13] The coronavirus spike (S) protein, comprising two subunits S1 and S2, plays a pivotal role in mediating viral entry.[14] Upon binding to the host ACE2 through its S1 subunit, the S protein undergoes dramatic conformational changes and proteolytic processing, triggering the S2 subunit to facilitate the fusion of viral and cellular membranes. The receptor binding domain (RBD) at the tip of the S1 subunit directly interacts with the protease domain of ACE2, which locates at the top-middle part of the ACE2 ectodomain.[15,16] The crystal structure of the RBD bound with human ACE2 reveals a gently concave surface, which cradles the N-terminal helix of ACE2.[17]

ACE2 is a type I transmembrane glycoprotein ubiquitously expressed in mammalian tissues, prominently in lung, heart, kidney, and intestine.[18] It functions as a carboxypeptidase and plays an important role in the renin-angiotensin system (RAS), a key regulator of systemic blood pressure and renal function.[19] The extracellular domain of ACE2 comprises a peptidase domain (Q18-A614) and a collectrin-like domain (D615-S740). Shedding can be mediated by metalloprotease ADAM17 and transmembrane protease serine 2 (TMPRSS2), and the resulting soluble ACE2 (sACE2) retains its catalytic activity and binding ability to the spike proteins.[20,21] Hence, recombinant sACE2 has been explored as a potential therapeutic option for COVID-19.

Lei et al. demonstrated the neutralization of SARS-CoV and SARS-CoV-2 pseudotyped viruses using wild-type (WT) sACE2 with reduced catalytic activity and observed inhibition of viral-infection-induced cell fusion.[22] Another human WT sACE2 protein, APN-01 (Apeiron Biologics), was clinically tested for acute respiratory distress syndrome (ARDS)[23] and demonstrated safety and tolerability in COVID-19 patients in the phase I study.[24] However, in the subsequent phase II study (NCT04335136), it failed to demonstrate significantly improved clinical outcomes in the treatment of severely ill COVID-19 patients, although improvements in mechanical ventilator-free days among surviving patients and a reduction in viral RNA load were observed.[25] Several factors likely contribute to the limited efficacy of WT sACE2 in patients. These factors include the rapid clearance of WT sACE2 from the body and the often-elevated level of endogenous sACE2s in severe COVID-19 cases,[26,27] which compete with WT sACE2 for binding to the spike protein.

Given that WT ACE2 binds to the SARS-CoV-2 spike RBD with only modest affinity,[10,28,29] employing engineered ACE2 proteins with enhanced binding affinity against RBDs could substantially augment neutralization potency, as evidenced by the *in vitro* and *in vivo* studies.[13,15,30–36] One promising strategy involves constructing recombinant ACE2 as a multivalent decoy, which results in significantly improved binding avidity and a prolonged circulating half-life.[13,30] An alternative approach to engineer ACE2 includes introducing key mutations to optimize its binding affinity against SARS-CoV-2 RBD. Various experimental approaches, such as random mutagenesis and deep mutagenesis, have been employed to generate ACE2 mutant libraries displayed on mammalian or yeast cells. These libraries were then screened for SARS-CoV-2 RBD binding, and high-affinity ACE2 binders were identified using fluorescence-activated cell sorting (FACS) and deep sequencing.[15,32,36] In addition to experimental techniques, computational modeling and simulation of the interactions between SARS-CoV-2 RBD and ACE2 have been used to identify hot-spot residues and predict substitutions that confer enhanced binding affinity.[31,34,35,37–39] These insights from computational analyses can be complemented by experimental protein engineering strategies, combining both approaches for further screening and/or affinity maturation of the engineered ACE2.[31] It is of note that, to date, all reported strategies for developing optimized ACE2 mutants have primarily focused on enhancing the interaction between ACE2 and SARS-CoV-2 RBD.

In this study, we present an innovative strategy to design and develop a universal ACE2 decoy receptor for the neutralization of ACE2-associated coronaviruses. Given that both SARS-CoV and SARS-CoV-2 utilize ACE2 as their entry point, we first constructed homology models of the native human ACE2-SARS-CoV RBD and ACE2-SARS-CoV-2 RBD complexes, modeling the single RBD/ACE2 protein complex (one RBD vs. one ACE2) in each case. Through *in silico* site saturation mutagenesis (SSM), we predicted key ACE2 residues interacting with the RBDs of both coronaviruses. Subsequently, saturation mutagenesis was executed for each identified key residue using molecular cloning and protein engineering methods. Individual mutations with increased affinity were identified via kinetic binding assessment against SARS-CoV and SARS-CoV-2 RBDs concurrently, and combinations of the mutation were also assessed. Here, we report the identification and characterization of the triple mutant ACE2-YHA and discuss its potential as a universal therapeutics to treat a wide range of ACE2-mediated coronavirus infections.

RESULTS

Native ACE2–RBD complex structure, organization, and interaction surface

The N-terminal helix of ACE2's extracellular domain directly contacts the S protein RBD surface (Figure 1A). High-resolution X-ray structures of human ACE2 bound to SARS-CoV/SARS-CoV-2 RBD reveal an uneven hydrogen bonding network bolstered by few hydrophobic interactions dispersed across the interface surface (Figure 1B). More extensive hydrogen bonding occurs toward the C-terminus of the N-terminal helix, whereas the N-terminus is anchored by a single H-bond only in the SARS-CoV-2 ACE2-RBD structure (Figure 1B, bottom left and bottom right). The N-terminus of ACE2's N-terminal helix interacts with SARS-CoV RBD exclusively via hydrophobic interaction. In both variants, a triad of hydrophobic RBD residues

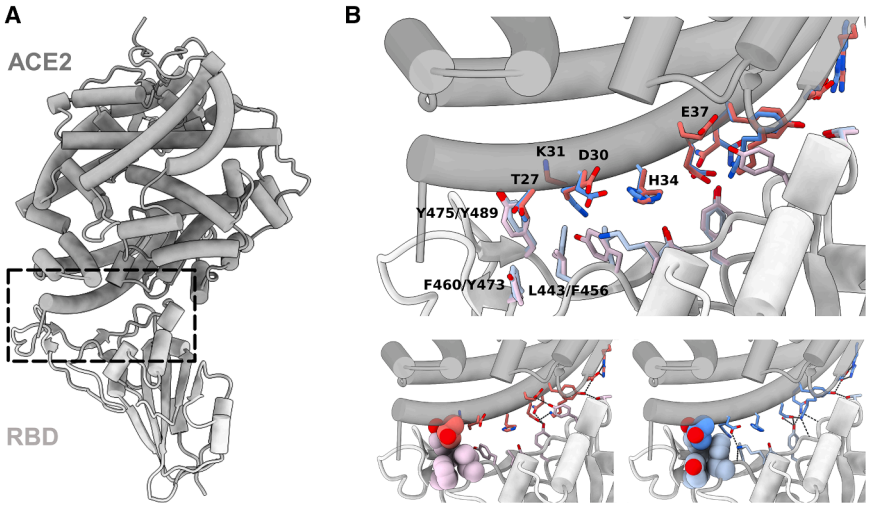

Figure 1. Native human ACE2–SARS-CoV/SARS-CoV-2 complex

(A) The extracellular domain of ACE2 shown in dark gray is bound to the receptor binding domain of SARS-CoV-2 (light gray). Image created from PDB: 6M0J. The complex interface is outlined.

(B) (Top) The interface in detail. ACE2/SARS-CoV residues are colored red and pink, respectively, while ACE2/SARS-CoV-2 residues are presented in blue and light blue. Image was created from PDB: 2AJF and 6M0J. Key residues that factor prominently in *in silico* SSM analysis are highlighted with bold text. (Bottom left) The native interactions of ACE2 with SARS-CoV RBD consist of weak hydrophobic interactions between ACE2 T27 and RBD L443, F460, and Y475 and several hydrogen bonds formed between the C-terminus of ACE2's N-terminal helix and the RBD. (Bottom right) Native interactions of ACE2 bound to SARS-CoV-2 RBD are largely similar to those of SARS-CoV albeit with a greater number and distribution of hydrogen bonds and slightly more satisfied hydrophobic interactions between ACE2 T27 and RBD F456, Y473, and Y489.

(L443, F460, and Y475 in SARS-CoV RBD and F456, Y473, and Y489 in SARS-CoV-2 RBD) forms a pocket that is partially filled by the γ carbon of ACE2 T27 (Figure 1B). As such, the ACE2 N-terminus region appears to be weakly bound to the SARS-CoV RBD and SARS-CoV-2 RBD, making it an optimal target for affinity and kinetics optimization.

Design of high-affinity ACE2 decoys by computational prediction

Our *in silico* approach of optimizing ACE2–RBD interaction is described in Materials and Methods and illustrated in Figure 2. Single-site *in silico* SSM identified six RBD-interacting ACE2 residues, T27, F28, K31, H34, Y41, and Q42, that increase complex stability beyond 10% (Table S1). It has been reported that T27, F28, K31, H34, and Y41 are located at the ACE2/RBD interface with distances of less than 4 Å for both SARS-CoV and SARS-CoV-2, whereas Q42 is involved in polar inter-protein interactions.[7] A linear increase in the calculated complex stability of double, triple, quadruple, and quintuple mutant combinations was observed for each additional site evaluated (Table S2). However, the absolute stability of a 6-mutant construct consisting of all six high-scoring ACE2 sites was computed to be approximately 13% and 4% lower than the most stable 5- and 4-mutant constructs, respectively, suggesting the interface surface can tolerate a maximum number of changes with diminishing returns in stability occurring beyond that limit.

Generation and analysis of ACE2 single-residue mutation

We first constructed the recombinant human ACE2-Fc fusion protein by fusing the entire ACE2 ectodomain (Q18-S740) to the N-terminus of a human IgG1 Fc domain. A prior study demonstrated that ACE2-Fc fusion proteins containing full-length ACE2 ectodomain is more effective than those containing only peptidase domain in blocking viral infection.[13] Concerns about the systemic administration of ACE2 includes the potential influence in the balance of the renin-angiotensin system (RAS), which may affect the therapeutic index. To address this, we introduced the R273Q/H505L mutation to the enzyme active site, which is outside the RBD binding region, to diminish ACE2's catalytic activity.[40] Kinetic binding data showed that this mutation did not alter ACE2's binding affinity to RBD (Figure S1).

To determine whether replacing amino acids at the six identified high-scoring ACE2 residue sites could improve ACE2–RBD binding affinity, we conducted single-site saturation mutagenesis (excluding mutations to cysteine) employing WT ACE2-Fc R273Q/H505L as the template. The ACE2 variants were generated using the transient ExpiCHO expression system, and the crude supernatant containing ACE2-Fc variants was tested directly with biolayer interferometry (BLI) assay for high-throughput screening. Prior to the binding assay, the supernatant was examined with SDS-PAGE. Successful expression was observed for all mutations at the T27, K31, H34, and Q42 sites. However, mutations in F28 and Y41 resulted in poor protein expression (Figure S2). This outcome suggests that mutations in F28 and Y41 may compromise the stability of ACE2. Notably, a multiple sequence alignment of over 200 ACE2 sequences derived from mammals reveals that F28 and Y41 are relatively conserved sites.[35] Given the pivotal role of protein stability in ACE2 engineering for therapeutic purposes, it is important to exclude unstable mutation sites in the early stage of selection. The supernatant obtained from the mock transfection lacked detectable ACE2-Fc protein and showed no binding signal in the BLI assays.

Single amino acid alterations in ACE2-Fc that resulted in enhanced binding to the RBDs of SARS-CoV and SARS-CoV-2 were observed in the BLI assays (Figure 3; Table S3). Notably, T27 mutations showed a broad-based improvement in RBD binding. Among them, T27Y, the second-best variant predicted to increase ACE2–RBD complex stability (Table S1), demonstrated the highest binding affinity against both SARS-CoV and

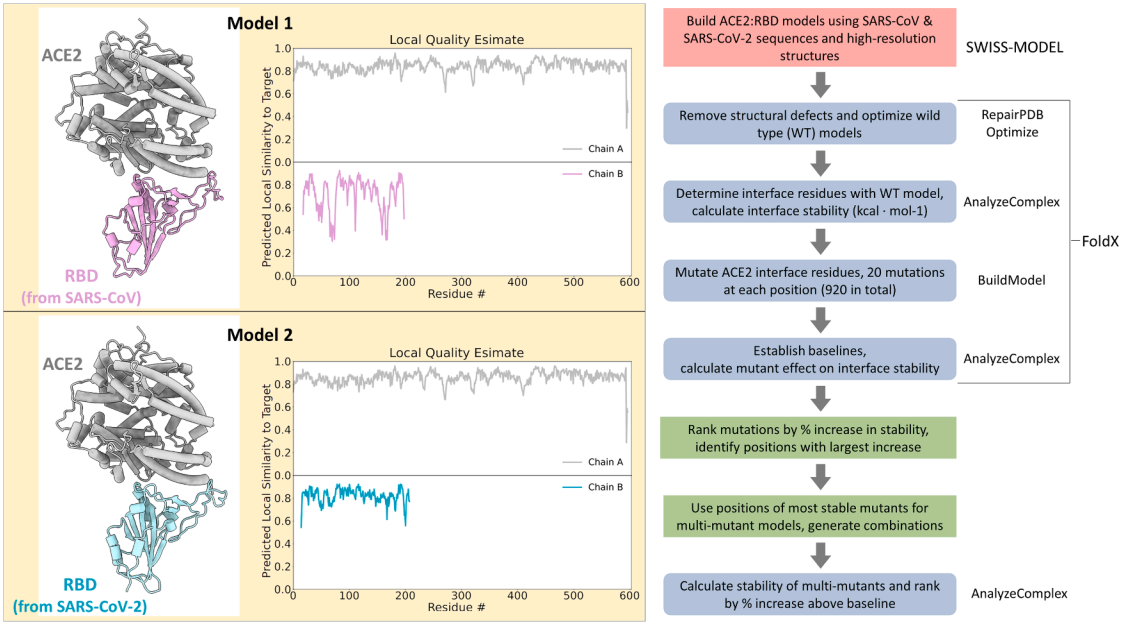

Figure 2. *In silico* SSM protocol

Flow chart detailing the *in silico* SSM pipeline described in the Materials and Methods. The modeling step (via SWISS-MODEL) is show in red, all steps requiring the FoldX 5.0 suite are blue, and in-house scripting and analysis steps are green.

SARS-CoV-2 RBDs. At the K31 site, mutations improved ACE2 binding against SARS-CoV RBD but not SARS-CoV-2 RBD. The top-performing variants for binding to both RBDs were the highest-scoring K31Y in increasing complex stability (Table S1) and the K31H that displayed the lowest off rate in SARS-CoV RBD binding (Table S3). Regarding the H34 mutation, H34 A/V exhibits superior SARS-CoV-2 RBD binding compared to the *in silico* high-scoring H34F, with SARS-CoV binding remaining unchanged (Figure 3). Q42 mutations, along with the few successfully expressed F28 and Y41 variants, demonstrated dissociation rates near or worse than WT ACE2 and were excluded from the multi-mutant analysis.

In summary, the F28, Y41, and Q42 sites were ruled out due to their adverse effects on protein expression and kinetic binding. Previous *in silico* studies indicated that the most significant in complex stability occurs between the K31Y-H34F double mutant and the Q42K single mutant, allotting an additional 14% increase in stability (Tables S1 and S2). Besides, the broad-spectrum potency was observed at the T27 site in kinetic binding assays, which prompts consideration of a T27-K31-H34 triple site construct. Given the binding affinity for both SARS-CoV and SARS-CoV-2 RBDs, T27Y, K31H/Y, and H34 A/V were selected for the multi-mutant analysis.

Triple-mutant combination improves binding affinity for SARS-CoV and SARS-CoV-2

We incorporated the selected single mutants T27Y, K31H/Y, and H34 A/V in the ACE2-Fc R273Q/H505L format and generated purified triple-mutant ACE2-Fc variants for kinetic binding assessment. The results revealed that all triple-mutant combinations, T27Y/K31H/H34A (YHA), T27Y/K31H/H34V (YHV), T27Y/K31Y/H34A (YYA), and T27Y/K31Y/H34V (YYV), significantly improved ACE2's binding affinity against both SARS-CoV and SARS-CoV-2 RBDs (Figure 4). The optimal variant, ACE2-YHA, bound to SARS-CoV RBD and SARS-CoV-2 RBD with KD values 0.75 nM and 1.69 nM, respectively, which is 55-fold and 11-fold reduction compared to the WT ACE2 binding. The K31H mutation demonstrated superior improvement in binding affinity against SARS-CoV RBD compared to K31Y, whereas the H34A mutation outperformed H34V in enhancing SARS-CoV-2 RBD binding in the triple-mutant combination.

Structural basis for improved ACE2-YHA RBD binding

Figure 5 details the interaction surfaces of the native ACE2-SARS-CoV-2 RBD and ACE2-YHA-SARS-CoV-2 RBD complexes. Space-filling representations illustrate a loose interaction between native ACE2 residues and a hydrophobic RBD triad formed by residues F456, Y473, and Y489, whereas the H34 side chain obstructs close hydrophobic association of Y453 and L455 in the RBD binding loop (Figure 5A). Increased RBD affinity observed in ACE2-YHA binding assays is driven by the planar side chains of Y27 and H31, resulting in greater hydrophobic and stacking interactions (Figure 5B). Furthermore, the removal of H34's bulky side chain via mutation to alanine allows for tighter association in the YHA triple mutant.

Structural alignment of the crystal structures of the human ACE2-SARS-CoV-2 Delta (B.1.617.2) variant RBD complex (PDB: 7W9I) and the equine ACE2-SARS-CoV-2 Omicron BA.1 (B.1.1.529.1) variant RBD complex (PDB: 7XBY) with the ACE2-YHA-WT SARS-CoV-2 RBD model reveals a highly consistent ACE2-RBD contact surface, particularly around the ACE2 N-terminal region, where the effects of amino acid

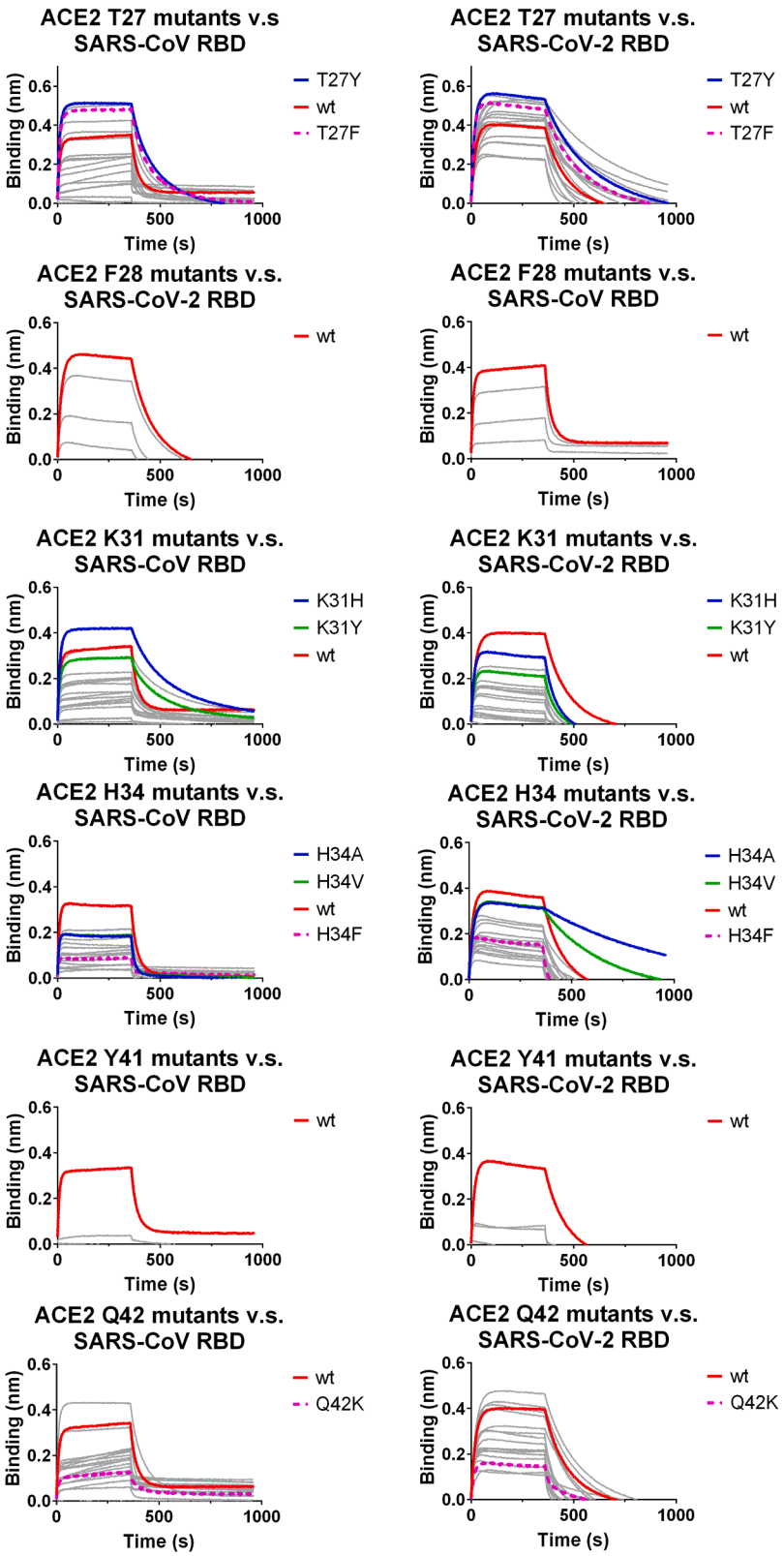

Figure 3. Kinetic binding of ACE2 single mutants

Binding and dissociation of ACE2 mutant variants to and from immobilized SARS-CoV and SARS-CoV-2 RBDs by BLI. The supernatant of ExpiCHOs transiently expressing ACE2-Fc variants was used directly for the binding test. Selected variants for further study were shown in solid line, and the top variants from the *in silico* approach were shown in dashed lines. No accurate KD for crude supernatant test as the protein concentration is unknown. See also Table S3.

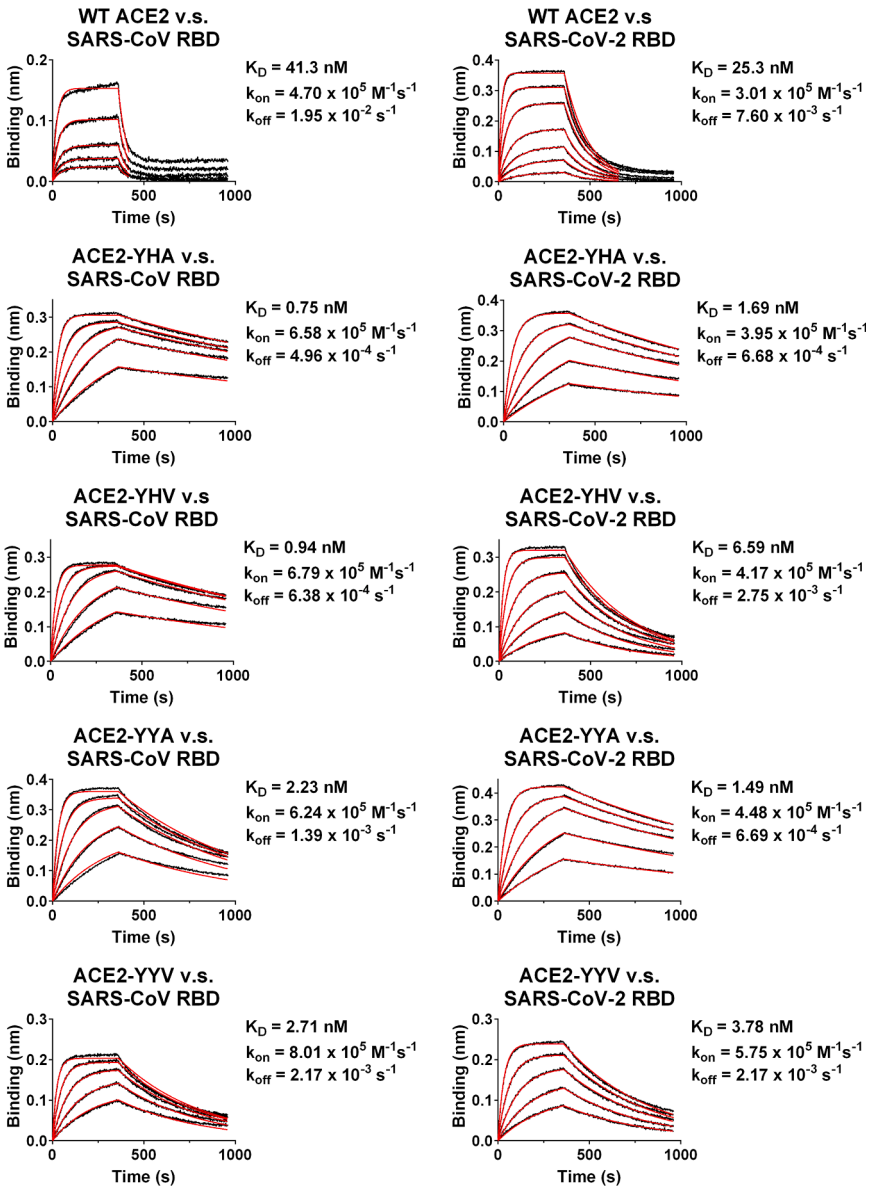

Figure 4. ACE2 triple mutant affinity measurement against MBP-SARS-CoV RBD and MBP-SARS-CoV-2 RBD

Binding affinity of ACE2-Fc triple mutant and wild-type ACE2 to SARS-CoV and SARS-CoV-2 spike RBD proteins was measured by BLI assay. All the variants and the wild-type (WT) ACE2 shown here have R273Q/H505L mutation in ACE2. Immobilized ACE2-Fc binding to the RBDs was tested using a range of MBP-RBD concentrations from 200 nM to 3,125 nM (in 2-fold dilution).

substitutions were examined (Figures 1B and S3).[41,42] Notably, both variants exhibit precisely the same RBD residues that adopt rotameric conformations nearly identical to those of the WT RBD, suggesting that the ACE2-YHA-variant RBD interactions are likely to be highly similar, if not identical, to those observed in the WT structure (Figures 1B and S3).[41,42]

Neutralization of SARS-CoV and SARS-CoV-2 variants by ACE2 decoys

The neutralizing potential of purified ACE2-Fc variants against pseudotyped SARS-CoV and SARS-CoV-2 viruses was assessed. The engineered Chinese hamster ovary (CHO) cells expressing human ACE2 served as the target cells for viral entry. In general, the binding affinity of the ACE2-Fc variants exhibited a correlation with their neutralization potency. Although the three single-mutant ACE2-Fc variants and the WT ACE2-Fc showed the ability to neutralize the pseudotyped viruses, their effectiveness varied across different SARS-CoV-2 variants (Figures 6A and 6B). ACE2-YHA consistently maintained high neutralizing potency against a broad spectrum of SARS-CoV-2 variants and SARS-CoV, with IC50 ranging from double-digit pM to sub-nM in most instances (Figures 6B and 6C). Particularly noteworthy was its significantly improved efficacy against SARS-CoV and some SARS-CoV-2 variants, such as E406W, E406W/D614G, and F486A, showcasing nearly a 10-fold reduction in IC50 compared to WT ACE2.

In a previous study, we developed an anti- SARS-CoV-2 RBD antibody 5A6, which exhibited robust neutralizing activity against pseudotyped and authentic SARS-CoV-2 viruses.[4] However, certain SARS-CoV-2 variants demonstrated resistance to 5A6 IgG (Figure 6B). On the other hand, ACE2-YHA consistently outperformed WT ACE2 in neutralizing all tested pseudoviruses, even though it might not reach the potency of 5A6 in certain scenarios. We further tested ACE2-YHA against recent Omicron variants, including the recombinant XBB lineage. These tests revealed that ACE2-YHA effectively neutralizes the pseudoviruses of the currently circulating Omicron variants (Figure 6C).

ACE2-YHA demonstrates high-affinity binding to bat coronaviruses

We further tested the binding affinity of ACE2-YHA across five bat SARS-like coronavirus strains: LYRa11, Rs4084, Rs4231, Rs7327, and RsSCH014. The RBD sequences of LYRa11 and Rs7327 closely resemble that of SARS-CoV,[43,44] whereas Rs4231, RsSHC014, and Rs4084 exhibited more genetic differences from SARS-CoV in the RBD region.[44] Notably, pseudotyped viruses expressing the spikes of Rs7327, Rs4231, and RsSHC014 could be replicated in human ACE2-expressing cells.[44,45] For the kinetic binding assay, we produced the

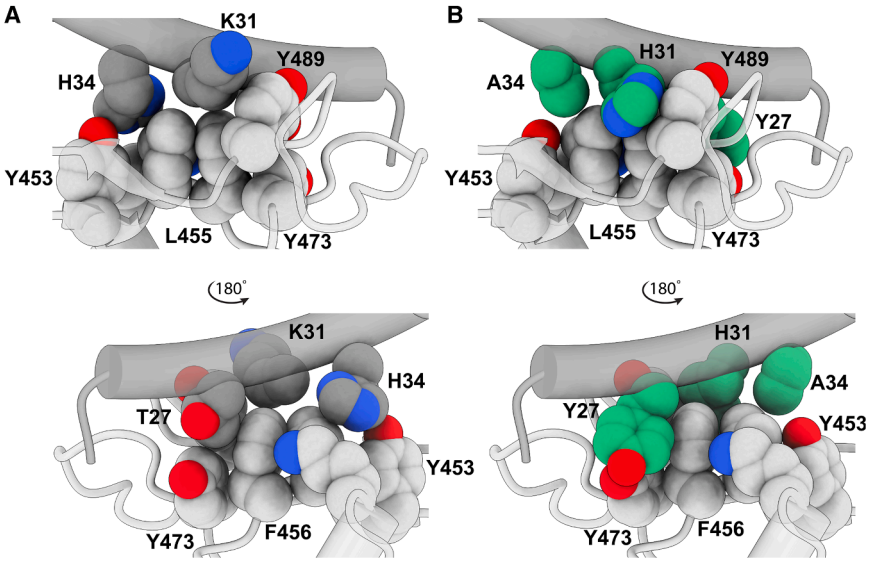

Figure 5. ACE2/RBD interaction surface

(A) A space-filling view of native ACE2 interactions with SARS-COV-2 RBD. WT ACE2 residues T27/K31/H34 are shown in dark gray, and the SARS-CoV-2 RBD residues are shown in light gray.

(B) Interactions of the YHA triple mutants (residues shown in green) with the SARS-CoV-2 RBD. The red and blue dots represent oxygen and nitrogen, respectively.

RBDs of these coronaviruses fused to the C-terminal of MBP proteins. ACE2-YHA showed a 1.9- to 2.7-fold improvement in binding affinity compared to WT ACE2 (Table 1). Previous studies have demonstrated that recombinant WT ACE2 can block the cell entry of pseudotyped viruses of these five strains.[46] This suggests that our engineered ACE2-YHA, with its enhanced binding affinity, is poised to exert cross-CoV neutralizing effects.

ACE2-YHA fully neutralizes SARS-CoV-2 infection in human airway epithelia

To further assess the antiviral potential of ACE2-YHA, we finally evaluated its capacity to halt infection by two clinically relevant and antigenically distant SARS-CoV-2 viruses, namely Delta (B.1.617.2) and Omicron (BA.5), in live virus assays using a reconstituted human airway epithelium (HAE) model. The predictive value of this model for the evaluation of antiviral candidates has been extensively described by our team and others.[47,48] B.1.617.2 or BA.5 SARS-CoV-2 viruses were preincubated for 60 min with 250 ng/mL of ACE2-WT or ACE2-YHA decoys before infection of MucilAir nasal HAE. Viral replication and tissue integrity were monitored daily by RT-qPCR and transepithelial electrical resistance (TEER), respectively, and compared to those of untreated controls. Infection resulted in high viral replication in the untreated control groups for both variants, with median apical viral titers of 9.16×10^5, 9.12×10^6, and 6.76×10^6 viral genome copies/mL at 24, 48, and 72 h post-infection (hpi) for B.1.617.2 and 1.95×10^6, 3.33×10^7, and 1.48×10^7 viral genome copies/mL for BA.5, respectively (Figures 7A and 7B). As expected, infection also negatively impacted the barrier function of the HAE, as shown by a marked drop in TEER values at 72 hpi for both viruses that already started at 48 hpi in the case of BA.5 (Figures 7C and 7D). Treatment with ACE2-WT did not confer any apparent benefit compared to the untreated controls, showing comparable median apical viral titers and the same TEER profile. Conversely, treatment with ACE2-YHA significantly neutralized SARS-CoV-2 infection, inducing >2.5 log10 and >3.5 log10 reductions on B.1.617.2 and BA.5 median apical viral genome copies/mL at 24 hpi, respectively. This neutralizing effect was further amplified to >5 log10 at 48 and 72 hpi, with all B.1.617.2 replicates and two out of four BA.5 replicates falling below the limit of quantification. Accordingly, the strong inhibition of SARS-CoV-2 infection by ACE2-YHA treatment also resulted in the protection of the airway epithelium integrity, as showed by the conservation of TEER values all throughout the viral infection kinetics. Altogether, these results demonstrate the capacity of engineered ACE2-YHA decoys to broadly neutralize antigenically distant SARS-CoV-2 viruses in the human airway epithelium.

DISCUSSION

In our pursuit to enhance human ACE2's neutralizing capability against a spectrum of ACE2-using coronaviruses, we employed a homology model of ACE2–SARS-CoV RBD/SARS-CoV-2 RBD complex. Through *in silico* SSM, we predicted critical ACE2-RBD interacting residues. Subsequently, we validated these predictions through experiments to assess the binding affinities of ACE2 mutants against SARS-CoV and SARS-CoV-2 RBDs in parallel. This comprehensive approach allowed us to identify optimal amino acid replacements for ACE2 engineering.

Achieving cross-species neutralization breadth requires the consideration of the diversity in how different coronaviruses engage ACE2. Despite the close phylogenetic relationship between SARS-CoV and SARS-CoV-2, their RBDs exhibit only 74% amino acid sequence identity.[49,50] Notably, SARS-CoV-2 RBD demonstrates higher hACE2 binding affinity than SARS-CoV RBD.[51] Our study revealed that certain single ACE2 mutations improved SARS-CoV RBD binding but adversely affected SARS-CoV-2 RBD binding and vice versa (Table S3). For instance, the K31H mutation favored SARS-CoV RBD binding, whereas the H34 mutants exhibited superior binding with SARS-CoV-2 RBD but not SARS-CoV (Figure 3). We opted for K31H as it offers a more comprehensive binding profile due to its strengthened engagement with SARS-CoV, compared to variants such as K31N, K31M, K31F, or K31W that were identified in studies focusing on SARS-CoV-2 engagement.[15,31,36,39,52–54] Our approach underscores the importance of considering RBDs from different coronaviruses to achieve an optimal

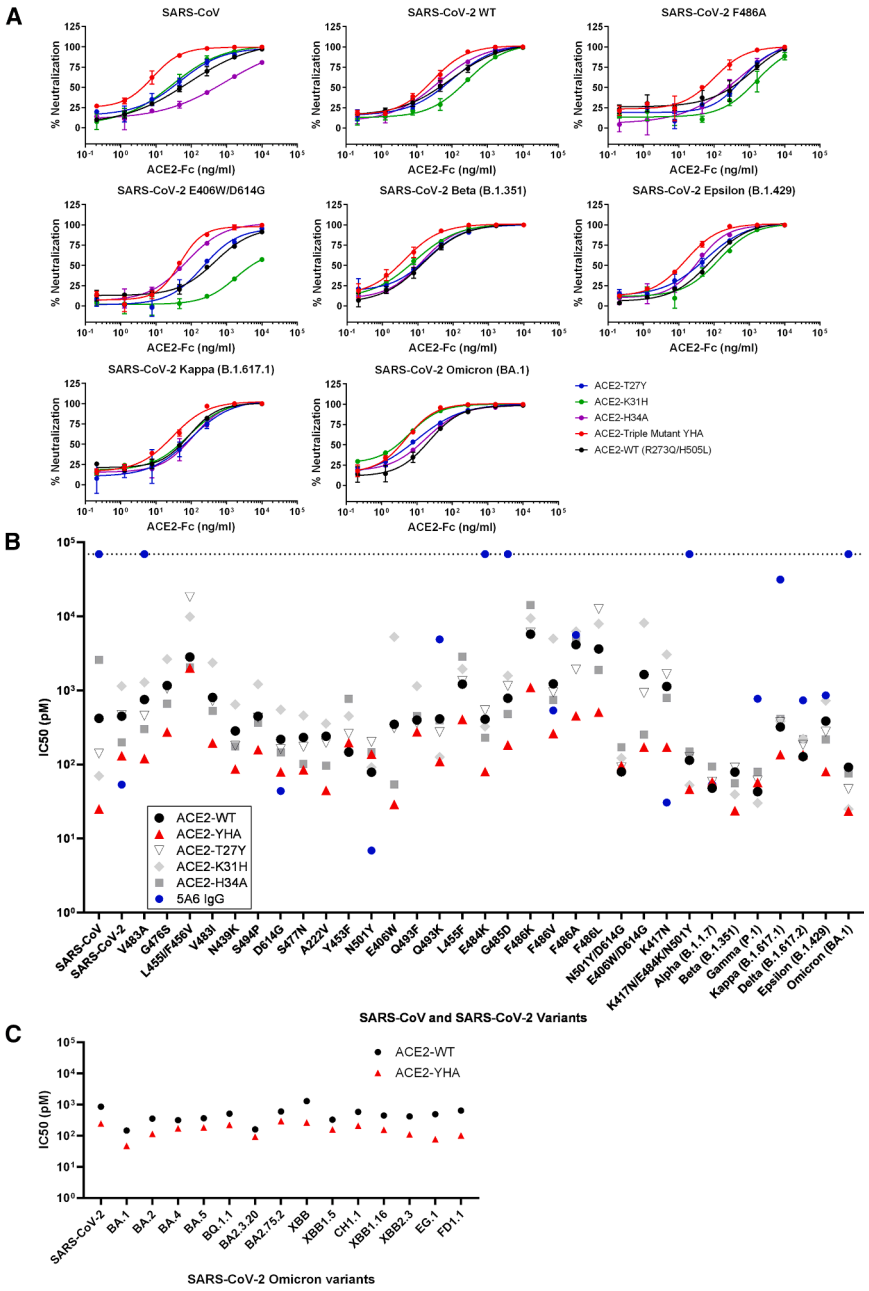

Figure 6. Neutralization of SARS-CoV and SARS-CoV-2 pseudoviruses

(A and B) Infection of CHO-ACE2 cells by SARS-CoVs pseudoviruses were determined in the presence of ACE2 variants. Luciferase activities in the CHO-ACE2 cells were measured, and the percent neutralization was calculated. The neutralization curves of some test results are shown in (A) to exhibit the dose-dependent neutralization of ACE2-Fc variants. Data are presented as mean ± SD in duplicates and are representative of two independent experiments. The IC50 was calculated by a variable slope four-parameter non-linear regression model using Graphpad PRISM 7 Software. Average IC50 of ACE2 mutant variants against WT SARS-CoV, WT SARS-CoV-2, and 31 variants of SARS-CoV-2 from two independent experiments are shown in (B). The dot line showed the limitation of detection (no neutralization).

(C) Neutralization of pseudoviruses representing various recent Omicron lineage variants of SARS-CoV-2. Average IC50 of ACE2-WT and ACE2-YHA are shown against WT SARS-CoV-2 and 14 Omicron variants from two independent experiments. All the ACE2 variants and ACE2-WT shown here have R273Q/H505L mutation in ACE2.

combination of amino acid replacement for designing a potent ACE2 universal decoy. By combining the optimal single mutations, we identified a triple-mutant ACE2, ACE2-YHA, which exhibited significantly improved RBD binding affinity to both SARS-CoV and SARS-CoV-2. Importantly, ACE2-YHA demonstrated cross-CoV binding activities beyond SARS-CoV and SARS-CoV-2, showcasing its potential as a versatile therapeutic candidate for fast responses against emerging outbreaks and pandemics. To provide a comprehensive overview of previously investigated ACE2 mutants and their binding and neutralization properties, Table 2 compares the mutants from the literature with our ACE2-YHA.

Several studies have employed 3D computational modeling of the SARS-CoV-2 spike RBD and ACE2 receptor complex to investigate how RBD mutations affect ACE2 binding, enhancing our understanding of the viral infectivity of SARS-CoV-2 variants of concern and predicting the binding affinity of neutralizing antibodies.[16,62,63] In contrast, other works, including ours, leverage this modeling approach alongside alternative strategies to identify key interface residues in ACE2 and predict mutations that may enhance its binding to the SARS-CoV-2 spike RBD[31,35,55,61,64] (Table 2). Our *in silico* analysis successfully discovered key residues—T27, K31, and H34—that are critical for high RBD-ACE2 binding affinity, a finding supported by our *in vitro* SSM. The highest affinity ACE2 mutant predicted by *in silico* mutagenesis was T27F-K31Y-H34F, which showed the greatest increase in complex stability compared to WT ACE2 (Table S2). Although the sequences differ, the amino acid substitutions of the best *in vitro* mutant, T27Y-K31H-H34A, share similar physicochemical properties (e.g., steric bulk, planarity, and hydrophobicity) with those of the highest-performing *in silico* model (Figure S4). The positions of ACE2 residues identified by our computational model were validated through targeted *in vitro* SSM, demonstrating the potential of our approach in narrowing down critical residues and streamlining the experimental process. Discrepancies between the computational and the *in vitro* results

Table 1. ACE2 triple mutant affinity measurement against bat CoV RBDs

	ACE2-YHA-Fc			WT ACE2-Fc		
Antigen	KD (nM)	Kon (1/Ms)	koff (1/s)	KD (nM)	Kon (1/Ms)	Koff (1/s)
MBP-LYRa11-RB	5.95	1.15E+06	6.85E-03	11.1	8.75E+05	9.72E-03
MBP-Rs4084-RBD	9.38	9.35E+05	8.77E-03	23.3	4.22E+05	9.83E-03
MBP-Rs4231-RBD	8.69	1.20E+06	1.04E-02	20.8	4.46E+05	9.26E-03
MBP-Rs7327-RBD	7.94	1.24E+06	9.86E-03	21.8	6.40E+05	1.40E-02
MBP-RsSCH014-RBD	9.25	1.11E+06	1.03E-02	24.2	4.23E+05	1.02E-02
MBP-SARS-CoV RBD	0.754	6.58E+05	4.96E-04	41.3	4.70E+05	1.95E-02
MBP-SARS-CoV-2 RBD	1.65	4.78E+05	7.90E-04	24.4	3.12E+05	7.62E-03

suggest there are limitations in the FoldX force field that do not sufficiently capture *in vitro* protein dynamics and binding kinetics. Our computational predictions are based on *in situ* protein complexes, which do not account for the kinetics and thermodynamics of complex formation, both at protein contact surfaces and allosteric sites. These dynamic factors influence binding affinity in experimental settings, underscoring the importance of experimental validation to capture the full spectrum of physicochemical and biological phenomena that govern protein stability and binding. By incorporating experimental data into the computational model, we may further refine predictions of key residues for designing ACE2 decoys that target a broader range of ACE2-utilizing coronaviruses, leveraging AI in drug discovery.

Our *in silico* modeling and experimental assessments of binding affinity were performed on a 1:1 interaction between RBDs and ACE2. However, the spike protein on the virus is trimeric, enabling multiple interactions with ACE2 receptors. Each of the three RBDs in the spike trimer can bind ACE2 independently,[31] and two trimeric spike proteins can simultaneously bind to an ACE2 homodimer.[16] Although native ACE2 is typically considered a monomeric receptor on the host cell surface, it may form dimers through its collectrin-like domain.[16] Therefore, the ACE2-Fc dimer could potentially

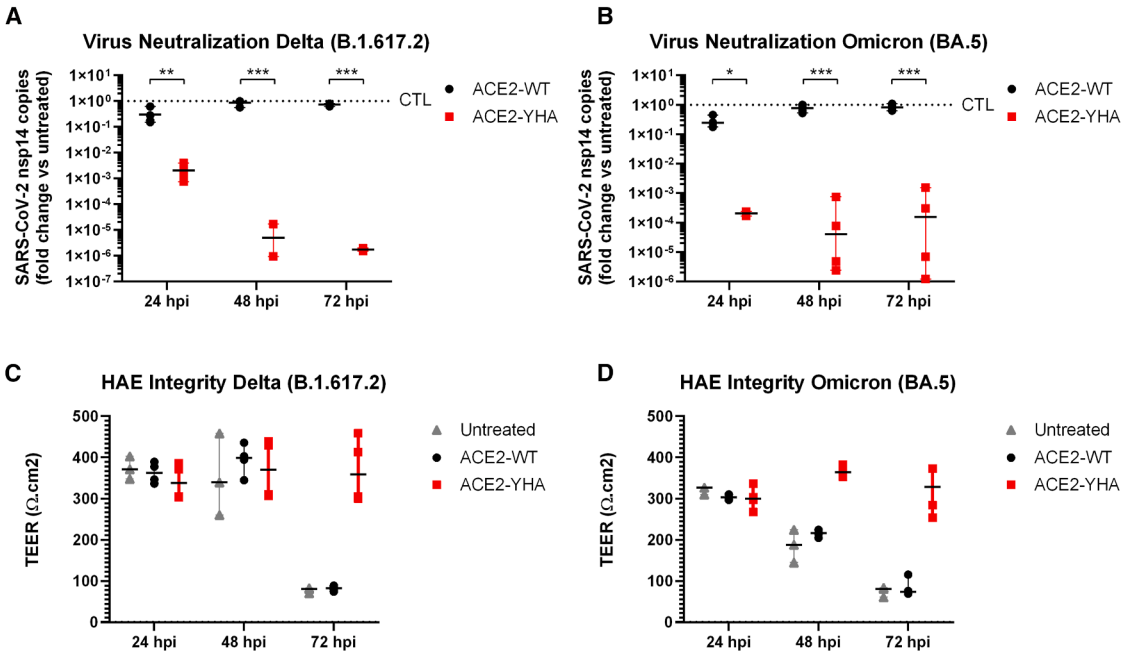

Figure 7. Engineered ACE2-YHA decoy protects human airway epithelium from infection with antigenically distant SARS-CoV-2 viruses

MucilAir nasal HAE were infected with B.1.617.2 (MOI 0.01) or BA.5 (MOI 0.001) SARS-CoV-2 viruses previously preincubated for 60 min with 250 ng/mL of ACE2-WT or ACE2-YHA decoys.

(A and B) Relative apical viral titers as determined by RT-qPCR and expressed in fold change of nsp14 copies compared to the infected untreated control (CTL, dotted line).

(C and D) Transepithelial electrical resistance (TEER) between the apical and basal poles of the HAE. *$p < 0.05$, **$p < 0.01$, and ***$p < 0.001$ indicate statistically significant differences in viral load between groups, determined by two-way analysis of variance (ANOVA) with Bonferroni post-test, performed using Graphpad PRISM 7 Software. Data are presented as median with range, based on four biological replicates per treatment condition ($n = 4$) and three replicates for the mock controls ($n = 3$). Each replicate corresponds to a single individual Transwell insert.

Table 2. Investigated ACE2 mutants and their binding properties

Mutations	Name	Format	Affinity against SARS-CoV RBD (nM)		Affinity against SARS-CoV-2 RBD (nM)		SARS-CoV pseudovirus neutralization IC50 (pM)		SARS-CoV-2 pseudovirus neutralization IC50 (pM)		Publications
			WT ACE2	ACE2 mutant	WT ACE2	ACE2 mutant	WT ACE2	ACE2 mutant	WT ACE2	ACE2 mutant	
Y27, H31, A34, Q273, L505	ACE2-YHA	sACE2-IgG1	41.3	0.8	24.4	1.7	422	24	454	128	Our work
F27, L42, I79, F330	FFWF/FLIF	sACE2-IgG1	NT	NT	8.2 (Delta)	0.1 (Delta)	345	46	309	36.5	Havranek et al.[38,55]; Islam et al.[56]
Y27, T79, Y330	sACE2v2.4	sACE2-IgG1	58	2.1	16	0.4	NT	NT	NT	NT	Chan et al.[32,33]; Zhang et al.[57,58]
L27, E30, R42, R79, R92, F330, L375		sACE2-IgG1	5.9–43.5	0.16–6.8	0.5–9	0.03	NT	NT	63930	3650	Cohen-Dvashi et al.[35]
V25, N31, K35, F79	3N39v4-Fc	sACE2-IgG1	NT	NT	NT	NT	1320	60	2320	188	Higuchi et al.[15]; Ikemura et al.[52]; Urano et al.[53]
M31, K35, A47, F79, P91, Y330		sACE2-IgG4	100	0.3	29	0.03	NT	94	NT	193	Sims et al.[36,54]
Y27, A34, 374N		sACE2-IgG1	NT	NT	21.4	0.56	NT	NT	8490	563	Tanaka et al.[34]
E24, K27, S34, E49, D90		sACE2-IgG1	NT	NT	11.6	5.5	45600	$>10^6$	11870	2470	Mou et al.[59]
F31, D33, S34, Q35	CVD313	sACE2-IgG1	15	3.9	3	NT	NT	NT	3240	128	Glasgow et al.[31]
19W, 330Y		sACE2-IgG1	NT	NT	4.7	0.5	21950	1790	7580	474	Ye et al.[60]
79F, 82Y, 325Y	M81	sACE2-IgG1	126	17.4	26	2.74	NT	NT	21230	2920	Chen et al.[61]

NT, not tested.

mimic the interactions between the ACE2 dimer and the spike protein. A study examining binding interactions between different multimeric forms of Spike-RBD and ACE2 revealed that although both ACE2 monomers and ACE2-Fc dimers can bind the isolated Spike-RBD, only the ACE2-Fc dimer binds tightly to the trimeric spike ectodomain and is more effective at neutralizing the virus.[65] This suggests that the ACE2-Fc dimer's higher intramolecular avidity enhances its binding affinity and makes it a more effective design than the monomer for blocking spike RBD's interactions with native ACE2. Additionally, the RBD in the spike's S1 subunit exists in two states: an inactive ''down'' state and an active ''up'' state, with only the ''up'' state capable of binding to ACE2. The spike protein typically has one RBD in the ''up'' state and two in the ''down'' state. The aforementioned study showed that a single spike protein can interact with multiple ACE2-Fc dimers simultaneously, suggesting that more than one RBD can adopt the ''up'' state, allowing multiple ACE2-Fc molecules to bind a single spike.[65]

Looking ahead, our strategy can be extended to include more coronaviruses known to use hACE2 as an entry receptor, such as the human alphacoronavirus NL63, thereby further broadening the binding breadth of the ACE2 decoy. This approach could be adopted to design decoys against other viruses such as Mpox, influenza, HIV, and Ebola. Moreover, recent advancements in novel ACE2 decoy formats, such as the immunoglobulin M (IgM)-like inhalable molecule HH-120,[66] hold promise for improved neutralization activity. Such formats can be integrated into our universal decoy for enhanced efficacy, representing a valuable avenue for future research and therapeutic development.

Limitations of the study

In this study, we focused solely on the interactions between ACE2 and SARS-CoV, as well as ACE2 and SARS-CoV-2, to predict and identify key ACE2-RBD interacting residues and mutations that could enhance the binding affinity of the ACE2 decoy. As a result, the improvements in affinity and neutralization may not apply to all ACE2-utilizing coronaviruses. To address this limitation, our approach could be expanded to include additional coronaviruses that use hACE2 as an entry receptor, such as the human alphacoronavirus NL63, thereby further broadening the binding spectrum of the ACE2 decoy.

RESOURCE AVAILABILITY

Lead contact

Further information and requests for resources and reagents should be directed to and will be fulfilled by the lead contact, Cheng-I Wang (Wang_ChengI@immunol.a-star.edu.sg).

Materials availability

All requests for resources and reagents should be directed to and will be fulfilled by the lead contact. All the ACE2 variants are proprietary and can be obtained through a Materials Transfer Agreement. Other materials will also be available from the lead contact with a completed Materials Transfer Agreement.

Data and code availability

- This paper analyzes existing, available data from the Protein DataBank, specifically: PDB ID 7W9I (https://doi.org/10.2210/pdb7W9I/pdb), PDB ID 7XBY (https://doi.org/10.2210/pdb7XBY/pdb), PDB ID 2AJF (https://doi.org/10.2210/pdb2AJF/pdb), and PDB ID 6M0J (https://doi.org/10.2210/pdb6M0J/pdb).
- This paper does not report original code.
- Any additional information required to reanalyze the data reported in this paper is available from the lead contact upon request.

ACKNOWLEDGMENTS

We thank Professor Yee-Joo Tan (Department of Microbiology, NUS; Institute of Molecular and Cell Biology, A*STAR) who kindly provided CHO-ACE2 cells and pXJ3′-S plasmid. We also thank Dr. Brendon Hanson (DSO National Laboratories) for providing pTT5LnX-coV-SP plasmid.

This work was supported through Biomedical Research Council (BMRC) COVID-19 research fund H20/04/g1/005 (R.G.H., C.I.W.) and Ministry of Health (MOH) Programme for Research in Epidemic Preparedness and REsponse (PREPARE) fund PREPARE-OC-VT-2022-001 (M.Z.T., R.G.H., C.I.W.). The computational work for this article was partially performed on resources of the National Supercomputing Centre, Singapore (https://www.nscc.sg).

AUTHOR CONTRIBUTIONS

C.Y.L., C.W.H., L.D.F., B.W., R.A.M., M.Z.T., M.R.C., A.P., R.G.H., and C.I.W. conceptualized and designed the study. M.Z.T., M.R.C., A.P., R.G.H., and C.I.W. supervised the study. C.Y.L., L.D.F., R.A.M., A.T., S.N.M.S., E.Z.X.N., Y.H., and J.K. conducted the experiments. C.Y.L., C.W.H., L.D.F., R.A.M., A.T., M.Z.T., and A.P. analyzed and interpreted the data. C.W.H., L.D.F., B.W., M.Z.T., M.R.C., A.P., R.G.H., and C.I.W. wrote, reviewed, and edited the manuscript. All authors read and approved the final manuscript.

DECLARATION OF INTERESTS

C.Y.L., C.W.H., L.D.F., R.A.M., B.W., R.G.H., and C.I.W. are listed as inventors of a filed patent for all the ACE2 variants mentioned in this manuscript. The other authors declare no competing interests.

DECLARATION OF GENERATIVE AI AND AI-ASSISTED TECHNOLOGIES IN THE WRITING PROCESS

During the preparation of this work, the author(s) used ChatGPT in the writing process to improve the readability and language of the manuscript. After using this tool, the author(s) carefully reviewed and edited the content as needed and take(s) full responsibility for the content of the publication.

STAR★METHODS

Detailed methods are provided in the online version of this paper and include the following:

- KEY RESOURCES TABLE
- EXPERIMENTAL MODEL AND STUDY PARTICIPANT DETAILS
  - Cells
  - Human airway epithelia (HAE)
- METHOD DETAILS
  - ACE2–RBD complex homology modeling
  - ACE2–RBD complex parametrization and equilibration
  - In silico optimization of ACE2–RBD interaction
  - ACE2 mutant generation and high throughput screening
  - Recombinant protein production
  - Affinity measurement by BioLayer interferometry (BLI)
  - Generation of pseudovirus particles expressing SARS-CoV-2 spike glycoprotein
  - ACE2 neutralization assay with SARS-CoV-2 or SARS-CoV spike glycoprotein pseudovirus
  - ACE2 neutralization assay with SARS-CoV-2 virus in reconstituted human airway epithelia (HAE)
- QUANTIFICATION AND STATISTICAL ANALYSIS

SUPPLEMENTAL INFORMATION

Supplemental information can be found online at https://doi.org/10.1016/j.isci.2025.112687.

Received: September 4, 2024
Revised: February 17, 2025
Accepted: May 14, 2025
Published: May 16, 2025

REFERENCES

1. Garcia-Beltran, W.F., Lam, E.C., St Denis, K., Nitido, A.D., Garcia, Z.H., Hauser, B.M., Feldman, J., Pavlovic, M.N., Gregory, D.J., Poznansky, M. C., et al. (2021). Multiple SARS-CoV-2 variants escape neutralization by vaccine-induced humoral immunity. Cell *184*, 2372–2383.e9. https://doi.org/10.1016/j.cell.2021.03.013.
2. Planas, D., Veyer, D., Baidaliuk, A., Staropoli, I., Guivel-Benhassine, F., Rajah, M.M., Planchais, C., Porrot, F., Robillard, N., Puech, J., et al. (2021). Reduced sensitivity of SARS-CoV-2 variant Delta to antibody neutralization. Nature *596*, 276–280. https://doi.org/10.1038/s41586-021-03777-9.
3. Starr, T.N., Greaney, A.J., Addetia, A., Hannon, W.W., Choudhary, M.C., Dingens, A.S., Li, J.Z., and Bloom, J.D. (2021). Prospective mapping of viral mutations that escape antibodies used to treat COVID-19. Science *371*, 850–854. https://doi.org/10.1126/science.abf9302.
4. Asarnow, D., Wang, B., Lee, W.H., Hu, Y., Huang, C.W., Faust, B., Ng, P. M.L., Ngoh, E.Z.X., Bohn, M., Bulkley, D., et al. (2021). Structural insight into SARS-CoV-2 neutralizing antibodies and modulation of syncytia. Cell *184*, 3192–3204.e16. https://doi.org/10.1016/j.cell.2021.04.033.
5. Tragni, V., Mercurio, I., Paoletti, D.P., Onofrio, A., Laera, L., Cafferati Beltrame, L., Sgobba, M.N., Guerra, L., Volpicella, M., De Grassi, A., et al. (2023). Deconstructing SARS-CoV-2 neutralization: A modular molecular framework for computational design and comparison of antibodies and nanobodies targeting the spike RBD. J. Med. Virol. *95*, e28875. https://doi.org/10.1002/jmv.28875.
6. Pierri, C.L. (2020). SARS-CoV-2 spike protein: flexibility as a new target for fighting infection. Signal Transduct. Target. Ther. *5*, 254. https://doi.org/10.1038/s41392-020-00369-3.
7. Mercurio, I., Tragni, V., Busto, F., De Grassi, A., and Pierri, C.L. (2021). Protein structure analysis of the interactions between SARS-CoV-2 spike protein and the human ACE2 receptor: from conformational changes to novel neutralizing antibodies. Cell. Mol. Life Sci. *78*, 1501–1522. https://doi.org/10.1007/s00018-020-03580-1.
8. Valério, M., Borges-Araújo, L., Melo, M.N., Lousa, D., and Soares, C.M. (2022). SARS-CoV-2 variants impact RBD conformational dynamics and ACE2 accessibility. Front. Med. Technol. *4*, 1009451. https://doi.org/10.3389/fmedt.2022.1009451.
9. Hoffmann, M., Kleine-Weber, H., Schroeder, S., Krüger, N., Herrler, T., Erichsen, S., Schiergens, T.S., Herrler, G., Wu, N.H., Nitsche, A., et al. (2020). SARS-CoV-2 Cell Entry Depends on ACE2 and TMPRSS2 and Is Blocked by a Clinically Proven Protease Inhibitor. Cell *181*, 271–280.e8. https://doi.org/10.1016/j.cell.2020.02.052.
10. Walls, A.C., Park, Y.J., Tortorici, M.A., Wall, A., McGuire, A.T., and Veesler, D. (2020). Structure, Function, and Antigenicity of the SARS-CoV-2 Spike Glycoprotein. Cell *181*, 281–292.e6. https://doi.org/10.1016/j.cell.2020.02.058.
11. Zhou, P., Yang, X.L., Wang, X.G., Hu, B., Zhang, L., Zhang, W., Si, H.R., Zhu, Y., Li, B., Huang, C.L., et al. (2020). A pneumonia outbreak associated with a new coronavirus of probable bat origin. Nature *579*, 270–273. https://doi.org/10.1038/s41586-020-2012-7.
12. Zheng, M., Zhao, X., Zheng, S., Chen, D., Du, P., Li, X., Jiang, D., Guo, J.T., Zeng, H., and Lin, H. (2020). Bat SARS-Like WIV1 coronavirus uses the ACE2 of multiple animal species as receptor and evades IFITM3 restriction via TMPRSS2 activation of membrane fusion. Emerg. Microbes Infect. *9*, 1567–1579. https://doi.org/10.1080/22221751.2020.1787797.
13. Li, Y., Wang, H., Tang, X., Fang, S., Ma, D., Du, C., Wang, Y., Pan, H., Yao, W., Zhang, R., et al. (2020). SARS-CoV-2 and Three Related Coronaviruses Utilize Multiple ACE2 Orthologs and Are Potently Blocked by an Improved ACE2-Ig. J. Virol. *94*, e01283-20. https://doi.org/10.1128/jvi.01283-20.
14. Tortorici, M.A., and Veesler, D. (2019). Structural insights into coronavirus entry. Adv. Virus Res. *105*, 93–116. https://doi.org/10.1016/bs.aivir.2019.08.002.
15. Higuchi, Y., Suzuki, T., Arimori, T., Ikemura, N., Mihara, E., Kirita, Y., Ohgitani, E., Mazda, O., Motooka, D., Nakamura, S., et al. (2021). Engineered ACE2 receptor therapy overcomes mutational escape of SARS-CoV-2. Nat. Commun. *12*, 3802. https://doi.org/10.1038/s41467-021-24013-y.
16. Yan, R., Zhang, Y., Li, Y., Xia, L., Guo, Y., and Zhou, Q. (2020). Structural basis for the recognition of SARS-CoV-2 by full-length human ACE2. Science *367*, 1444–1448. https://doi.org/10.1126/science.abb2762.
17. Li, F., Li, W., Farzan, M., and Harrison, S.C. (2005). Structure of SARS coronavirus spike receptor-binding domain complexed with receptor. Science *309*, 1864–1868. https://doi.org/10.1126/science.1116480.
18. Saponaro, F., Rutigliano, G., Sestito, S., Bandini, L., Storti, B., Bizzarri, R., and Zucchi, R. (2020). ACE2 in the Era of SARS-CoV-2: Controversies and Novel Perspectives. Front. Mol. Biosci. *7*, 588618. https://doi.org/10.3389/fmolb.2020.588618.
19. Hamming, I., Cooper, M.E., Haagmans, B.L., Hooper, N.M., Korstanje, R., Osterhaus, A.D.M.E., Timens, W., Turner, A.J., Navis, G., and van Goor, H. (2007). The emerging role of ACE2 in physiology and disease. J. Pathol. *212*, 1–11. https://doi.org/10.1002/path.2162.
20. Rahman, M.M., Hasan, M., and Ahmed, A. (2021). Potential detrimental role of soluble ACE2 in severe COVID-19 comorbid patients. Rev. Med. Virol. *31*, 1–12. https://doi.org/10.1002/rmv.2213.
21. Brest, P., Refae, S., Mograbi, B., Hofman, P., and Milano, G. (2020). Host Polymorphisms May Impact SARS-CoV-2 Infectivity. Trends Genet. *36*, 813–815. https://doi.org/10.1016/j.tig.2020.08.003.
22. Lei, C., Qian, K., Li, T., Zhang, S., Fu, W., Ding, M., and Hu, S. (2020). Neutralization of SARS-CoV-2 spike pseudotyped virus by recombinant ACE2-Ig. Nat. Commun. *11*, 2070. https://doi.org/10.1038/s41467-020-16048-4.
23. Pang, X., Cui, Y., and Zhu, Y. (2020). Recombinant human ACE2: potential therapeutics of SARS-CoV-2 infection and its complication. Acta Pharmacol. Sin. *41*, 1255–1257. https://doi.org/10.1038/s41401-020-0430-6.
24. Monteil, V., Kwon, H., Prado, P., Hagelkrüys, A., Wimmer, R.A., Stahl, M., Leopoldi, A., Garreta, E., Hurtado Del Pozo, C., Prosper, F., et al. (2020). Inhibition of SARS-CoV-2 Infections in Engineered Human Tissues Using Clinical-Grade Soluble Human ACE2. Cell *181*, 905–913.e7. https://doi.org/10.1016/j.cell.2020.04.004.
25. Arimori, T., Ikemura, N., Okamoto, T., Takagi, J., Standley, D.M., and Hoshino, A. (2022). Engineering ACE2 decoy receptors to combat viral escapability. Trends Pharmacol. Sci. *43*, 838–851. https://doi.org/10.1016/j.tips.2022.06.011.
26. Kragstrup, T.W., Singh, H.S., Grundberg, I., Nielsen, A.L.L., Rivellese, F., Mehta, A., Goldberg, M.B., Filbin, M.R., Qvist, P., and Bibby, B.M. (2021). Plasma ACE2 predicts outcome of COVID-19 in hospitalized patients. PLoS One *16*, e0252799. https://doi.org/10.1371/journal.pone.0252799.
27. Wallentin, L., Lindbäck, J., Eriksson, N., Hijazi, Z., Eikelboom, J.W., Ezekowitz, M.D., Granger, C.B., Lopes, R.D., Yusuf, S., Oldgren, J., and Siegbahn, A. (2020). Angiotensin-converting enzyme 2 (ACE2) levels in relation to risk factors for COVID-19 in two large cohorts of patients with atrial fibrillation. Eur. Heart J. *41*, 4037–4046. https://doi.org/10.1093/eurheartj/ehaa697.
28. Lan, J., Ge, J., Yu, J., Shan, S., Zhou, H., Fan, S., Zhang, Q., Shi, X., Wang, Q., Zhang, L., and Wang, X. (2020). Structure of the SARS-CoV-2 spike

receptor-binding domain bound to the ACE2 receptor. Nature *581*, 215–220. https://doi.org/10.1038/s41586-020-2180-5.

29. Obeng, E.M., Fianu, I., and Danquah, M.K. (2022). Multivalent ACE2 engineering-A promising pathway for advanced coronavirus nanomedicine development. Nano Today *46*, 101580. https://doi.org/10.1016/j.nantod.2022.101580.
30. Guo, L., Bi, W., Wang, X., Xu, W., Yan, R., Zhang, Y., Zhao, K., Li, Y., Zhang, M., Cai, X., et al. (2021). Engineered trimeric ACE2 binds viral spike protein and locks it in "Three-up" conformation to potently inhibit SARS-CoV-2 infection. Cell Res. *31*, 98–100. https://doi.org/10.1038/s41422-020-00438-w.
31. Glasgow, A., Glasgow, J., Limonta, D., Solomon, P., Lui, I., Zhang, Y., Nix, M.A., Rettko, N.J., Zha, S., Yamin, R., et al. (2020). Engineered ACE2 receptor traps potently neutralize SARS-CoV-2. Proc. Natl. Acad. Sci. USA *117*, 28046–28055. https://doi.org/10.1073/pnas.2016093117.
32. Chan, K.K., Dorosky, D., Sharma, P., Abbasi, S.A., Dye, J.M., Kranz, D.M., Herbert, A.S., and Procko, E. (2020). Engineering human ACE2 to optimize binding to the spike protein of SARS coronavirus 2. Science *369*, 1261–1265. https://doi.org/10.1126/science.abc0870.
33. Chan, K.K., Tan, T.J.C., Narayanan, K.K., and Procko, E. (2021). An engineered decoy receptor for SARS-CoV-2 broadly binds protein S sequence variants. Sci. Adv. *7*, eabf1738. https://doi.org/10.1126/sciadv.abf1738.
34. Tanaka, S., Nelson, G., Olson, C.A., Buzko, O., Higashide, W., Shin, A., Gonzalez, M., Taft, J., Patel, R., Buta, S., et al. (2021). An ACE2 Triple Decoy that neutralizes SARS-CoV-2 shows enhanced affinity for virus variants. Sci. Rep. *11*, 12740. https://doi.org/10.1038/s41598-021-91809-9.
35. Cohen-Dvashi, H., Weinstein, J., Katz, M., Eilon-Ashkenazy, M., Mor, Y., Shimon, A., Achdout, H., Tamir, H., Israely, T., Strobelt, R., et al. (2022). Anti-SARS-CoV-2 immunoadhesin remains effective against Omicron and other emerging variants of concern. iScience *25*, 105193. https://doi.org/10.1016/j.isci.2022.105193.
36. Sims, J.J., Greig, J.A., Michalson, K.T., Lian, S., Martino, R.A., Meggersee, R., Turner, K.B., Nambiar, K., Dyer, C., Hinderer, C., et al. (2021). Intranasal gene therapy to prevent infection by SARS-CoV-2 variants. PLoS Pathog. *17*, e1009544. https://doi.org/10.1371/journal.ppat.1009544.
37. Payandeh, Z., Rahbar, M.R., Jahangiri, A., Hashemi, Z.S., Zakeri, A., Jafarisani, M., Rasaee, M.J., and Khalili, S. (2020). Design of an engineered ACE2 as a novel therapeutics against COVID-19. J. Theor. Biol. *505*, 110425. https://doi.org/10.1016/j.jtbi.2020.110425.
38. Havranek, B., Chan, K.K., Wu, A., Procko, E., and Islam, S.M. (2021). Computationally Designed ACE2 Decoy Receptor Binds SARS-CoV-2 Spike (S) Protein with Tight Nanomolar Affinity. J. Chem. Inf. Model. *61*, 4656–4669. https://doi.org/10.1021/acs.jcim.1c00783.
39. Köchl, K., Schopper, T., Durmaz, V., Parigger, L., Singh, A., Krassnigg, A., Cespugli, M., Wu, W., Yang, X., Zhang, Y., et al. (2023). Optimizing variant-specific therapeutic SARS-CoV-2 decoys using deep-learning-guided molecular dynamics simulations. Sci. Rep. *13*, 774. https://doi.org/10.1038/s41598-023-27636-x.
40. Guy, J.L., Jackson, R.M., Jensen, H.A., Hooper, N.M., and Turner, A.J. (2005). Identification of critical active-site residues in angiotensin-converting enzyme-2 (ACE2) by site-directed mutagenesis. FEBS J. *272*, 3512–3520. https://doi.org/10.1111/j.1742-4658.2005.04756.x.
41. Wang, Y., Liu, C., Zhang, C., Wang, Y., Hong, Q., Xu, S., Li, Z., Yang, Y., Huang, Z., and Cong, Y. (2022). Structural basis for SARS-CoV-2 Delta variant recognition of ACE2 receptor and broadly neutralizing antibodies. Nat. Commun. *13*, 871. https://doi.org/10.1038/s41467-022-28528-w.
42. Xu, Z., Kang, X., Han, P., Du, P., Li, L., Zheng, A., Deng, C., Qi, J., Zhao, X., Wang, Q., et al. (2022). Binding and structural basis of equine ACE2 to RBDs from SARS-CoV, SARS-CoV-2 and related coronaviruses. Nat. Commun. *13*, 3547. https://doi.org/10.1038/s41467-022-31276-6.
43. He, B., Zhang, Y., Xu, L., Yang, W., Yang, F., Feng, Y., Xia, L., Zhou, J., Zhen, W., Feng, Y., et al. (2014). Identification of diverse alphacoronaviruses and genomic characterization of a novel severe acute respiratory syndrome-like coronavirus from bats in China. J. Virol. *88*, 7070–7082. https://doi.org/10.1128/jvi.00631-14.
44. Hu, B., Zeng, L.P., Yang, X.L., Ge, X.Y., Zhang, W., Li, B., Xie, J.Z., Shen, X.R., Zhang, Y.Z., Wang, N., et al. (2017). Discovery of a rich gene pool of bat SARS-related coronaviruses provides new insights into the origin of SARS coronavirus. PLoS Pathog. *13*, e1006698. https://doi.org/10.1371/journal.ppat.1006698.
45. Menachery, V.D., Yount, B.L., Jr., Debbink, K., Agnihothram, S., Gralinski, L.E., Plante, J.A., Graham, R.L., Scobey, T., Ge, X.Y., Donaldson, E.F., et al. (2015). A SARS-like cluster of circulating bat coronaviruses shows potential for human emergence. Nat. Med. *21*, 1508–1513. https://doi.org/10.1038/nm.3985.
46. Tada, T., Fan, C., Chen, J.S., Kaur, R., Stapleford, K.A., Gristick, H., Dcosta, B.M., Wilen, C.B., Nimigean, C.M., and Landau, N.R. (2020). An ACE2 Microbody Containing a Single Immunoglobulin Fc Domain Is a Potent Inhibitor of SARS-CoV-2. Cell Rep. *33*, 108528. https://doi.org/10.1016/j.celrep.2020.108528.
47. Pizzorno, A., Padey, B., Julien, T., Trouillet-Assant, S., Traversier, A., Errazuriz-Cerda, E., Fouret, J., Dubois, J., Gaymard, A., Lescure, F.X., et al. (2020). Characterization and Treatment of SARS-CoV-2 in Nasal and Bronchial Human Airway Epithelia. Cell Rep. Med. *1*, 100059. https://doi.org/10.1016/j.xcrm.2020.100059.
48. Maisonnasse, P., Guedj, J., Contreras, V., Behillil, S., Solas, C., Marlin, R., Naninck, T., Pizzorno, A., Lemaitre, J., Gonçalves, A., et al. (2020). Hydroxychloroquine use against SARS-CoV-2 infection in non-human primates. Nature *585*, 584–587. https://doi.org/10.1038/s41586-020-2558-4.
49. Tai, W., He, L., Zhang, X., Pu, J., Voronin, D., Jiang, S., Zhou, Y., and Du, L. (2020). Characterization of the receptor-binding domain (RBD) of 2019 novel coronavirus: implication for development of RBD protein as a viral attachment inhibitor and vaccine. Cell. Mol. Immunol. *17*, 613–620. https://doi.org/10.1038/s41423-020-0400-4.
50. Shang, J., Ye, G., Shi, K., Wan, Y., Luo, C., Aihara, H., Geng, Q., Auerbach, A., and Li, F. (2020). Structural basis of receptor recognition by SARS-CoV-2. Nature *581*, 221–224. https://doi.org/10.1038/s41586-020-2179-y.
51. Shang, J., Wan, Y., Luo, C., Ye, G., Geng, Q., Auerbach, A., and Li, F. (2020). Cell entry mechanisms of SARS-CoV-2. Proc. Natl. Acad. Sci. USA *117*, 11727–11734. https://doi.org/10.1073/pnas.2003138117.
52. Ikemura, N., Taminishi, S., Inaba, T., Arimori, T., Motooka, D., Katoh, K., Kirita, Y., Higuchi, Y., Li, S., Suzuki, T., et al. (2022). An engineered ACE2 decoy neutralizes the SARS-CoV-2 Omicron variant and confers protection against infection in vivo. Sci. Transl. Med. *14*, eabn7737. https://doi.org/10.1126/scitranslmed.abn7737.
53. Urano, E., Itoh, Y., Suzuki, T., Sasaki, T., Kishikawa, J.I., Akamatsu, K., Higuchi, Y., Sakai, Y., Okamura, T., Mitoma, S., et al. (2023). An inhaled ACE2 decoy confers protection against SARS-CoV-2 infection in preclinical models. Sci. Transl. Med. *15*, eadi2623. https://doi.org/10.1126/scitranslmed.adi2623.
54. Sims, J.J., Lian, S., Meggersee, R.L., Kasimsetty, A., and Wilson, J.M. (2022). High activity of an affinity-matured ACE2 decoy against Omicron SARS-CoV-2 and pre-emergent coronaviruses. PLoS One *17*, e0271359. https://doi.org/10.1371/journal.pone.0271359.
55. Havranek, B., Lindsey, G.W., Higuchi, Y., Itoh, Y., Suzuki, T., Okamoto, T., Hoshino, A., Procko, E., and Islam, S.M. (2023). A computationally designed ACE2 decoy has broad efficacy against SARS-CoV-2 omicron variants and related viruses in vitro and in vivo. Commun. Biol. *6*, 513. https://doi.org/10.1038/s42003-023-04860-9.
56. Islam, M.S., Havranek, B., Procko, E., and Chan, K. (2022). Computationally engineered ACE2 decoy binds with nanomolar affinity with the SARS-CoV-2 spike protein. Biophys. J. *121*, 422a. https://doi.org/10.1016/j.bpj.2021.11.664.
57. Zhang, L., Dutta, S., Xiong, S., Chan, M., Chan, K.K., Fan, T.M., Bailey, K.L., Lindeblad, M., Cooper, L.M., Rong, L., et al. (2022). Engineered ACE2 decoy mitigates lung injury and death induced by SARS-CoV-2 variants.

Nat. Chem. Biol. *18*, 342–351. https://doi.org/10.1038/s41589-021-00965-6.

58. Zhang, L., Narayanan, K.K., Cooper, L., Chan, K.K., Skeeters, S.S., Devlin, C.A., Aguhob, A., Shirley, K., Rong, L., Rehman, J., et al. (2022). An ACE2 decoy can be administered by inhalation and potently targets omicron variants of SARS-CoV-2. EMBO Mol. Med. *14*, e16109. https://doi.org/10.15252/emmm.202216109.
59. Mou, H., Quinlan, B.D., Peng, H., Liu, G., Guo, Y., Peng, S., Zhang, L., Davis-Gardner, M.E., Gardner, M.R., Crynen, G., et al. (2021). Mutations derived from horseshoe bat ACE2 orthologs enhance ACE2-Fc neutralization of SARS-CoV-2. PLoS Pathog. *17*, e1009501. https://doi.org/10.1371/journal.ppat.1009501.
60. Ye, F., Lin, X., Chen, Z., Yang, F., Lin, S., Yang, J., Chen, H., Sun, H., Wang, L., Wen, A., et al. (2021). S19W, T27W, and N330Y mutations in ACE2 enhance SARS-CoV-2 S-RBD binding toward both wild-type and antibody-resistant viruses and its molecular basis. Signal Transduct. Target. Ther. *6*, 343. https://doi.org/10.1038/s41392-021-00756-4.
61. Chen, Y., Sun, L., Ullah, I., Beaudoin-Bussières, G., Anand, S.P., Hederman, A.P., Tolbert, W.D., Sherburn, R., Nguyen, D.N., Marchitto, L., et al. (2022). Engineered ACE2-Fc counters murine lethal SARS-CoV-2 infection through direct neutralization and Fc-effector activities. Sci. Adv. *8*, eabn4188. https://doi.org/10.1126/sciadv.abn4188.
62. Deshpande, A., Harris, B.D., Martinez-Sobrido, L., Kobie, J.J., and Walter, M.R. (2021). Epitope Classification and RBD Binding Properties of Neutralizing Antibodies Against SARS-CoV-2 Variants of Concern. Front. Immunol. *12*, 691715. https://doi.org/10.3389/fimmu.2021.691715.
63. Tragni, V., Preziusi, F., Laera, L., Onofrio, A., Mercurio, I., Todisco, S., Volpicella, M., De Grassi, A., and Pierri, C.L. (2022). Modeling SARS-CoV-2 spike/ACE2 protein-protein interactions for predicting the binding affinity of new spike variants for ACE2, and novel ACE2 structurally related human protein targets, for COVID-19 handling in the 3PM context. EPMA J. *13*, 149–175. https://doi.org/10.1007/s13167-021-00267-w.
64. Sorokina, M., M C Teixeira, J., Barrera-Vilarmau, S., Paschke, R., Papasotiriou, I., Rodrigues, J.P.G.L.M., and Kastritis, P.L. (2020). Structural models of human ACE2 variants with SARS-CoV-2 Spike protein for structure-based drug design. Sci. Data *7*, 309. https://doi.org/10.1038/s41597-020-00652-6.
65. Irene Lui, X.X.Z., Lim, S.A., Elledge, S.K., Solomon, P., Rettko, N.J., Shoshana Zha, B., Kirkemo, L.L., Gramespacher, J.A., Liu, J., Muecksch, F., et al. (2020). Trimeric SARS-CoV-2 Spike interacts with dimeric ACE2 with limited intra-Spike avidity. Preprint at bioRxiv. https://doi.org/10.1101/2020.05.21.109157.
66. Liu, J., Mao, F., Chen, J., Lu, S., Qi, Y., Sun, Y., Fang, L., Yeung, M.L., Liu, C., Yu, G., et al. (2023). An IgM-like inhalable ACE2 fusion protein broadly neutralizes SARS-CoV-2 variants. Nat. Commun. *14*, 5191. https://doi.org/10.1038/s41467-023-40933-3.
67. Schymkowitz, J., Borg, J., Stricher, F., Nys, R., Rousseau, F., and Serrano, L. (2005). The FoldX web server: an online force field. Nucleic Acids Res. *33*, W382–W388. https://doi.org/10.1093/nar/gki387.
68. Ng, O.W., Keng, C.T., Leung, C.S.W., Peiris, J.S.M., Poon, L.L.M., and Tan, Y.J. (2014). Substitution at aspartic acid 1128 in the SARS coronavirus spike glycoprotein mediates escape from a S2 domain-targeting neutralizing monoclonal antibody. PLoS One *9*, e102415. https://doi.org/10.1371/journal.pone.0102415.
69. Gordon, J.C., Myers, J.B., Folta, T., Shoja, V., Heath, L.S., and Onufriev, A. (2005). H++: a server for estimating pKas and adding missing hydrogens to macromolecules. Nucleic Acids Res. *33*, W368–W371. https://doi.org/10.1093/nar/gki464.
70. Vanommeslaeghe, K., Hatcher, E., Acharya, C., Kundu, S., Zhong, S., Shim, J., Darian, E., Guvench, O., Lopes, P., Vorobyov, I., and Mackerell, A.D., Jr. (2010). CHARMM general force field: A force field for drug-like molecules compatible with the CHARMM all-atom additive biological force fields. J. Comput. Chem. *31*, 671–690. https://doi.org/10.1002/jcc.21367.
71. Waterhouse, A., Bertoni, M., Bienert, S., Studer, G., Tauriello, G., Gumienny, R., Heer, F.T., de Beer, T.A.P., Rempfer, C., Bordoli, L., et al. (2018). SWISS-MODEL: homology modelling of protein structures and complexes. Nucleic Acids Res. *46*, W296–W303. https://doi.org/10.1093/nar/gky427.
72. Guerois, R., Nielsen, J.E., and Serrano, L. (2002). Predicting changes in the stability of proteins and protein complexes: a study of more than 1000 mutations. J. Mol. Biol. *320*, 369–387. https://doi.org/10.1016/s0022-2836(02)00442-4.
73. Delgado, J., Radusky, L.G., Cianferoni, D., and Serrano, L. (2019). FoldX 5.0: working with RNA, small molecules and a new graphical interface. Bioinformatics *35*, 4168–4169. https://doi.org/10.1093/bioinformatics/btz184.

STAR★METHODS

KEY RESOURCES TABLE

REAGENT or RESOURCE	SOURCE	IDENTIFIER
Antibodies		
anti- SARS-CoV-2 RBD 5A6 IgG	Laboratory of Cheng-I Wang	N/A
Bacterial and virus strains		
SARS-CoV-2 Delta (B.1.617.2)	Laboratory of Andrés Pizzorno	EPI_ISL_7360393
SARS-CoV-2 Omicron (BA.5)	Laboratory of Andrés Pizzorno	EPI_ISL_15902382
Chemicals, peptides, and recombinant proteins		
ACE2-WT	Laboratory of Cheng-I Wang	N/A
ACE2-T27Y	Laboratory of Cheng-I Wang	N/A
ACE2-K31H	Laboratory of Cheng-I Wang	N/A
ACE2-H34A	Laboratory of Cheng-I Wang	N/A
ACE2-YHA	Laboratory of Cheng-I Wang	N/A
ACE2-YHV	Laboratory of Cheng-I Wang	N/A
ACE2-YYA	Laboratory of Cheng-I Wang	N/A
ACE2-YYV	Laboratory of Cheng-I Wang	N/A
MBP-LYRa11-RBD	Laboratory of Cheng-I Wang	N/A
MBP-Rs4084-RBD	Laboratory of Cheng-I Wang	N/A
MBP-Rs4231-RBD	Laboratory of Cheng-I Wang	N/A
MBP-Rs7327-RBD	Laboratory of Cheng-I Wang	N/A
MBP-RsSCH014-RBD	Laboratory of Cheng-I Wang	N/A
MBP- SARS-CoV RBD	Laboratory of Cheng-I Wang	N/A
MBP- SARS-CoV-2 RBD	Laboratory of Cheng-I Wang	N/A
PrimeSTAR Max DNA Polymerase PCR master mix	TaKaRa	Cat# R047A
QuikChange Lightning Multi Site-Directed Mutagenesis Kit	Agilent	Cat# 210513
OptiPrep (60% [wt/vol] iodixanol)	STEMCELL Technologies	Cat# 07820
Lipofectamine 2000 Transfection Reagent	Invitrogen	Cat# 11668-019
Dulbecco's modified Eagle's medium	Hyclone	Cat# SH30022.01
Fetal Bovine Serum (FBS)	GIBCO	Cat# 10270-106
Penicillin-Streptomycin	GIBCO	Cat# 15140-122
MEM Non-Essential Amino Acids Solution	GIBCO	Cat# 11140-050
Geneticin Selective Antibiotic (G418 Sulfate)	GIBCO	Cat# 10131-027
StemProTM AccutaseTM Cell Dissociation Reagent	GIBCO	Cat# A1110501
Critical commercial assays		
Lenti-X p24 rapid titer kit	Takara Bio	Cat# 632500
Luciferase Assay System	Promega	Cat# E1510
Experimental models: Cell lines		
ExpiCHO-S	Thermo Fisher Scientific	Cat# A29127
293T	ATCC	CRL-3216
CHO-ACE2	Laboratory of Yee-Joo Tan	Ng et al.[67]
MucilAir™ HAE	Epithelix SARL	MP0011

(*Continued on next page*)

Continued

REAGENT or RESOURCE	SOURCE	IDENTIFIER
Recombinant DNA		
Plasmid: pTT5	National Research Council of Canada	N/A
Plasmid: pcDNA3-LYRa11-RBD-8h	Addgene	Plasmid #161822
Plasmid: pcDNA3-Rs7327-RBD-8h	Addgene	Plasmid #161823
Plasmid: pcDNA3-Rs4231-RBD-8h	Addgene	Plasmid #161824
Plasmid: pcDNA3-Rs4084-RBD-8h	Addgene	Plasmid #161825
Plasmid: pcDNA3-RsSHC014-RBD-8h	Addgene	Plasmid #161826
Plasmid: pMDLg/pRRE	Addgene	Plasmid #12251
Plasmid: pRSV-Rev	Addgene	Plasmid #12253
Plasmid: pHIV-Luc-ZsGreen	Addgene	Plasmid #39196
Plasmid: pTT5LnX-coV-SP (codon optimized S gene of SARS-CoV-2, GenBank: YP_009724390.1)	DSO National Laboratories	N/A
Plasmid: pXJ3′-S (SARS-CoV spike protein from HKU39849 strain)	Professor Yee-Joo Tan	Ng et al.[68]
Software and algorithms		
SWISS-MODEL protein structure homology modeling server	SWISS-MODEL	https://swissmodel.expasy.org
H++ server (version 3.0)		Gordon et al.[69]
CHARMM36 force field		Vanommeslaeghe et al.[70]
GROMACS 2019.3	GROMACS	https://manual.gromacs.org/documentation/2019.3/user-guide/index.html
FoldX 5.0	FoldX	https://foldxsuite.crg.eu/
GraphPad Prism version 7.03	GraphPad	https://www.graphpad.com/; RRID: SCR_002798
Octet System Data Acquisition Software version 9.0.0.4.	ForteBio	N/A
Other		
10MWCO Vivaspin 20	Sartorius	Cat# VS2002
Protein G resin	Merck Millipore	Cat# 16-266
Ni-NTA agarose	Qiagen	Cat# 30210
SARS-CoV-2 Delta S-RBD-ACE2	Protein DataBank	PDB: 7W9I
The crystal structure of SARS-CoV-2 Omicron BA.1 variant RBD in complex with equine ACE2	Protein DataBank	PDB: 7XBY
Structure of SARS coronavirus spike receptor-binding domain complexed with its receptor	Protein DataBank	PDB: 2AJF
Crystal structure of SARS-CoV-2 spike receptor-binding domain bound with ACE2	Protein DataBank	PDB: 6M0J

EXPERIMENTAL MODEL AND STUDY PARTICIPANT DETAILS

Cells

The human embryonic kidney epithelial cell 293T (ATCC, CRL-3216) was cultured in Dulbecco's modified Eagle's medium (Hyclone, SH30022.01) supplemented with 10% heat-inactivated FBS (Gibco, 10270-106). A stable cell line expressing human ACE2, CHO-ACE2 (a kind gift from Professor Yee-Joo Tan, IMCB, A*STAR),[68] was maintained in Dulbecco's modified Eagle's medium supplemented with 10% heat-inactivated FBS, 1% MEM Non-Essential Amino Acids Solution (Gibco, 11140-050) and 0.5 mg/mL of GeneticinTM Selective Antibiotic (Gibco, 10131-027). Every 2–3 days, cells were passaged by dissociating the cells with StemPro Accutase Cell Dissociation Reagent (Gibco, A1110501).

Human airway epithelia (HAE)

MucilAir HAE reconstituted from human primary cells isolated and differentiated from nasal biopsies from a pool of 14 healthy donors (pool ref: MP0011) were provided by Epithelix SARL (Geneva, Switzerland) and maintained in air-liquid interphase with specific culture medium in Costar Transwell inserts (Corning, NY, USA), according to the manufacturer's instructions.

Unless otherwise stated, experiments using HAE were conducted in 4 biological replicates per treatment condition and 3 for mocks, each one in individual Transwell inserts. Samples were allocated to experimental groups based on treatment conditions and processed in parallel. No formal randomization was applied, as all samples were derived from the same donor pool batch and processed under identical conditions. Operators were blinded from group allocation during viral quantification.

METHOD DETAILS

ACE2–RBD complex homology modeling

We obtained structural models of the ACE2–RBD complex using the SWISS-MODEL protein structure homology modeling server (https://swissmodel.expasy.org), which helped model the missing residues 376–381 not present in structure PDB ID 2AJF[17] for the SARS-CoV RBD, and residues 319–332 and 527–541 not present in structure PDB ID 6M0J[28] for the SARS-CoV-2 RBD. Human ACE2 and SARS-CoV/SARS-CoV-2 RBD sequences were provided as targets for the initial template search. Templates derived from protein crystal structures of RBD-bound ACE2 complexes were filtered based on their global model quality estimate and selected for model building. We then prepared these models for *in silico* site saturation mutagenesis (SSM).

ACE2–RBD complex parametrization and equilibration

Protein complex models were submitted to the H++ server (version 3.0) to determine histidine residue protonation states at neutral pH.[69] All other ionizable residues were set to their default charged state. Protein complex parameters were derived using the CHARMM36 force field.[70] We solvated systems in 0.15 M sodium chloride solution containing approximately 77,000 TIP3P water molecules. Solvation resulted in cubic boxes of approximately $13.5 \times 13.5 \times 13.5$ nm. Subsequent equilibration of ACE2–RBD complexes was achieved by performing 5000 steps of steepest descent minimization followed by 200 ps *NpT* ensemble simulations with gradually decreasing position restraints on protein heavy atoms. An isotropic Berendsen barostat maintained a pressure of 1 atm, using a coupling constant τ of 2.0 ps. All simulation steps were performed using GROMACS 2019.3. Electrostatic interactions were described using particle mesh Ewald.[71] van der Waals and Ewald cut-offs were set to 1.2 nm. Bonds to hydrogen atoms were constrained with the LINCS algorithm, allowing an integration time step of 2 fs. Temperature was controlled for distinct coupling groups of solvent and solute using separate v-rescale thermostats[72] at 303.15 K, using a coupling constant τ of 1 ps.

In silico optimization of ACE2–RBD interaction

We processed equilibrated systems using FoldX 5.0's *RepairPDB* and *Optimize* routines before quantifying ACE2–RBD interaction energies.[67,73] These steps were performed to acclimate protein complexes within the FoldX force field and repair any remaining structural defects, i.e., specific residues with outlying torsion angles, significant clashes, and appreciable van der Waals strain. We then employed the *AnalyzeComplex* program to determine interacting ACE2 and RBD residues in native complex models. The list of ACE2 interface residues generated by *AnalyzeComplex* was fed into FoldX's *BuildModel* routine to perform *in silico* SSM resulting in approximately 800 single mutant ACE2–RBD models. We then used *AnalyzeComplex* again to assess the energetic contribution of single point mutations to protein complex stability by calculating the total free energy of ACE2–RBD interaction for each model. The free energy value for a given ACE2 residue mutated to itself was used as a baseline to calculate $\Delta\Delta$Gs resulting from all other point mutations at a specific site for the remaining 19 mutant complex models. This procedure allowed us to assess the effect of a single mutation on complex stability as the percentage change in interaction energy relative to baseline. We considered residue positions where mutations elicited a $\geq$10% increase in complex stability as high priority and ranked the mutations at these sites by magnitude. High scoring residue sites common to both models were collated and all possible permutations (2–6 simultaneous mutations) were used to generate multi-mutant models. We repeated the analysis process for the multi-mutant models and assessed their significance accordingly. The combination of residue positions from multi-mutant models yielding the largest increase in complex stability were the focus of *in vitro* SSM.

ACE2 mutant generation and high throughput screening

The ACE2-Fc variants with single mutation in the six predicted residue sites were constructed using two methods. The first method is linear DNA synthesis. A pTT5 vector (National Research Council of Canada) was constructed to contain the 5′-end protecting region, OriP, CMV promoter, signal peptide, wild-type ACE2-Fc gene, terminator, and 3′-end protecting region. The PrimeSTAR Max DNA Polymerase PCR master mix (TaKaRa) was used for PCR. DNA fragment A containing the 5′-end protecting region, OriP, CMV promoter, and signal peptide, and DNA fragment B containing the ACE2-Fc variants, terminator, and the 3′-end protecting region, were obtained from PCR using the constructed pTT5 vector as template. Site-saturation mutagenesis (SSM) was achieved by using the individual PCR primers which encode the 18 substitute amino acids (excluding Cysteine) at each position, respectively, when amplifying the fragment B. The assembled fragments were amplified again to obtain the complete linear PCR products for direct Expi-CHO transfection. The second method is to construct a similar pTT5-ACE2-Fc plasmid without OriP and introduce the ACE2 mutations by

using degenerate primers (NNK) for site-directed mutagenesis (QuikChange Lightning Multi Site-Directed Mutagenesis Kit, Agilent). DNA (plasmid or PCR fragment) was used to transfect Expi-CHO cells in 24-well plates. After 8-day expression, the supernatant was collected for the RBD binding test using BioLayer Interferometry (BLI) assay. For each batch of expression, WT ACE2 was included as positive control, and the mock transfection was done as negative control.

Recombinant protein production

The engineered ACE2-Fc constructs in the pTT5 vector (National Research Council of Canada) were expressed using ExpiCHO expression system (Thermo Fisher Scientific) with transient transfection. Eight days after transfection, ExpiCHO-S cell suspension was centrifuged for 10 min at 2000 rpm and filtered with 0.22 μm filter to remove the cells and debris. The engineered ACE2s were then purified from the culture supernatant using Protein G resin (Merck Millipore) following the manufacturer's instructions. After elution, the purified recombinant proteins were dialyzed at 4°C for 4–20 h against 1x PBS, for 3 times and concentrated to 1–2 mg/mL using 10MWCO Vivaspin 20 (Sartorius).

The RBDs of SARS-CoV, SARS-CoV-2, and five SARS-like CoVs from Rhinolophus bat species (isolates LYRa11, Rs4084, Rs4231, Rs7327, RsSHC014, plasmids obtained from Addgene, ID 161822–161826)[33] were constructed in the pTT5 vector. To enhance the RBD production, Maltose binding protein (MBP) was added to the N-terminal of RBD,[33] following a His-tag and followed by a TEV cleavage site before the RBD constructs. The fusion proteins were expressed in ExpiCHO system as described above and purified using Ni-NTA agarose (Qiagen) following the manufacturer's instructions. After elution, the purified recombinant proteins were dialyzed at 4°C for 4–20 h against 1x PBS for 3 times and concentrated to 1–2 mg/mL using 10MWCO Vivaspin 20 (Sartorius).

Affinity measurement by BioLayer interferometry (BLI)

Binding affinity of the ACE2-containing supernatant or purified ACE2 variants to RBDs was measured on the Octet96Red system (ForteBio). Anti-human IgG Fc (AHC) sensors were first loaded with neat supernatant or 1 μg/mL of purified ACE2 mutant for 10 min, followed by kinetics buffer (phosphate-buffered saline buffer supplemented with 0.1% Tween 20 and 0.1% BSA) for 5 min to establish a stable baseline. The sensors were then dipped into RBDs from 200 nM to 3.125 nM in 2-fold dilutions for 6 min for testing the purified ACE2s (200 nM RBDs for testing the ACE2s in supernatant), and then in kinetics buffer again for 10 min to measure association and dissociation. Assays were run at 25°C and data was analyzed on the Octet System Data Acquisition Software version 9.0.0.4. using the 1:1 Langmuir binding model.

Generation of pseudovirus particles expressing SARS-CoV-2 spike glycoprotein

Pseudotyped viral particles expressing SARS-CoV-2 or SARS-CoV spike proteins were produced by transfecting of 30 million 293T cells with 12 μg pMDLg/pRRE (Addgene #12251), 6 μg pRSV-Rev (Addgene #12253), 24 μg pHIV-Luc-ZsGreen (Addgene #39196) and 12 μg pTT5LnX-coV-SP (expressing SARS-CoV-2 spike proteins, GenBank: YP_009724390.1, a kind gift from DSO National Laboratories) or 12 μg pXJ3′-S (expressing SARS-CoV spike protein from HKU39849 strain, a kind gift from Professor Yee-Joo Tan, IMCB, A*STAR)[68] using Lipofectamine 2000 transfection reagent (Invitrogen, 11668-019). The transfected cells were cultured at 37°C incubator for 3 days. Viral supernatant was harvested, centrifuged at 700 g for 10 min to remove cell debris and filtered through a 0.45 μm filter unit (Sartorius #16555). Lenti-X p24 rapid titer kit (Takara Bio, #632200) was used to quantify the viral titers following the manufacturer instructions. Plasmids for expressing SARS-CoV-2 spike protein mutants were generated using QuikChange Lightning Multi Site-Directed Mutagenesis Kit (Agilent, #210513).

ACE2 neutralization assay with SARS-CoV-2 or SARS-CoV spike glycoprotein pseudovirus

CHO-ACE2 cells were seeded at a density of 1.8 x 10^4 cells in 100 μL of complete medium without Geneticin in 96-well Flat Clear Bottom Black Polystyrene TC-treated Microplates (Corning, #3904) for overnight culture at 37°C incubator. Serially diluted ACE2-Fc proteins were incubated in a 96-well flat-bottom cell culture plate (Costar, #3596) with an equal volume of pseudovirus (6 ng of p24) at the final volume of 50 μL at 37°C for 1 h, and the mixture was added to the monolayer of pre-seeded CHO-ACE2 cells in triplicate. After 1 h of pseudovirus infection at 37°C, 150 μL of culture medium was added to each well and the cells were further incubated for another 48 h. Upon removal of culture medium, cells were washed with sterile PBS, and then lysed in 20 μL of 1x Passive lysis buffer (Promega, E1941) with gentle shaking at 37°C for 30 min. Luciferase activity was then assessed using a Luciferase Assay System (Promega, E1510) on a Promega GloMax Luminometer. The relative luciferase units (RLU) were converted to percent neutralization and plotted with a non-linear regression curve fit using PRISM.

ACE2 neutralization assay with SARS-CoV-2 virus in reconstituted human airway epithelia (HAE)

For neutralization experiments, the apical poles of HAE were gently washed twice with warm Opti-MEM medium (Gibco, ThermoFisher Scientific) and then infected with a 150 μL dilution of SARS-CoV-2 Delta (B.1.617.2, EPI_ISL_7360393) or Omicron (BA.5, EPI_ISL_15902382) in Opti-MEM medium, at a multiplicity of infection (MOI) of 0.01 or 0.001, respectively. Viral suspensions were pre-incubated 60 min at 37°C with 250 ng/mL of ACE2-WT or ACE2-YHA. Pre-incubation of the virus with Opti-MEM medium was used as untreated control. One-hour post-infection (hpi), the inoculum mix was removed from the apical pole and the HAE were incubated at 37°C and 5% CO2 for 72h. Variations in transepithelial electrical resistance (Δ TEER) were measured using a dedicated volt-ohm meter (EVOM2, Epithelial Volt/Ohm Meter for TEER) and expressed as Ohm/cm^2. At the indicated time points (24, 48, and

72 hpi), apical poles of the HAE were washed with warm OptiMEM, which was then collected for quantification of viral nsp14 gene copies by RT-qPCR as previously described.[47]

QUANTIFICATION AND STATISTICAL ANALYSIS

All statistical analyses were performed using GraphPad Prism version 7.03. Statistical tests used, exact *n* values, what n represents (e.g., number of independent biological replicates or wells), definitions of center (mean or median), and measures of variability or precision (SD or with range) are indicated in the figure legends, figures, and results section. IC50 values were calculated using the "[Inhibitor] vs. response - variable slope (four parameters)" nonlinear regression model in GraphPad Prism. Differences between experimental groups were analyzed using one-way or two-way ANOVA, as appropriate. Bonferroni post-tests were applied in live-virus neutralization assays using HAE. Differences were considered statistically significant at confidence levels $^{*}p < 0.05$ or $^{**}p < 0.01$, $^{***}p < 0.001$.